Published in final edited form as:
Biomaterials. 2013 September ; 34(28): 6615–6630. doi:10.1016/j.biomaterials.2013.05.033.

Imaging challenges in biomaterials and tissue engineering

Alyssa A. Appel[a,b], **Mark A. Anastasio**[c], **Jeffery C. Larson**[a,b], and **Eric M. Brey**[a,b,*]

[a]Department of Biomedical Engineering, Illinois Institute of Technology, 3255 South Dearborn St, Chicago, IL 60616, USA

[b]Research Service, Hines Veterans Administration Hospital, Hines, IL, USA

[c]Department of Biomedical Engineering, Washington University in St. Louis, St. Louis, MO, USA

Abstract

Biomaterials are employed in the fields of tissue engineering and regenerative medicine (TERM) in order to enhance the regeneration or replacement of tissue function and/or structure. The unique environments resulting from the presence of biomaterials, cells, and tissues result in distinct challenges in regards to monitoring and assessing the results of these interventions. Imaging technologies for three-dimensional (3D) analysis have been identified as a strategic priority in TERM research. Traditionally, histological and immunohistochemical techniques have been used to evaluate engineered tissues. However, these methods do not allow for an accurate volume assessment, are invasive, and do not provide information on functional status. Imaging techniques are needed that enable non-destructive, longitudinal, quantitative, and three-dimensional analysis of TERM strategies. This review focuses on evaluating the application of available imaging modalities for assessment of biomaterials and tissue in TERM applications. Included is a discussion of limitations of these techniques and identification of areas for further development.

Keywords

Image analysis; Molecular imaging; MRI (magnetic resonance imaging); Fluorescence; X-ray CT imaging

1. Introduction

Researchers in the fields of tissue engineering and regenerative medicine (TERM) are investigating new techniques for the regeneration, replacement and repair of lost or damaged tissues. These approaches are designed to restore tissue function and/or structure. While the specifics of a given strategy may vary, an approach typically involves some combination of biomaterials, cells, and inducible factors that are expected to generate tissues in bioreactors and/or following implantation *in vivo*. The unique environments resulting from interfaces between biomaterials, cells, and tissues found in TERM applications result in distinct challenges in regards to monitoring and assessing outcomes.

Imaging technologies for three-dimensional (3D) analysis have been identified as a strategic priority in TERM research and are required for acceleration of progress in the field [1]. Traditionally, histological and immunohistochemical techniques have been used to evaluate engineered tissues. However, these methods do not allow for an accurate volume assessment, are destructive, and do not provide information on functional status. There is a

*Corresponding author. Department of Biomedical Engineering, Illinois Institute of Technology, 3255 South Dearborn St, Chicago, IL 60616, USA. Tel.: +1 312 567 5098; fax: +1 312 567 5707. brey@iit.edu.

great need for the development and evaluation of 3D imaging tools that enable quantitative analysis of engineered tissues. Many imaging techniques exist, but when applied using standard methods may not provide the information required for assessment. The need for improved methods is well-known in the field, and researchers have begun to address some of the challenges. However, there has been little presentation in the literature of neither the unique aspects of this challenge nor discussion of the advantages/disadvantages of existing methods and those under development. In this paper we seek to present these issues as a means of guidance and for promoting discussion amongst researchers in the fields of biomaterials and TERM.

1.1. Imaging tasks

The primary imaging challenges in TERM depend, in part, on the therapeutic approach under investigation. While there is significant variability within a given approach, they can be placed in four generic categories as related to imaging needs (Fig. 1): 1) Regeneration that is based exclusively on the transplantation or injection of cells. The cells can be isolated from a variety of sources, can be a combination of multiple cell types, and may be modified in some way (e.g. gene transfer). Regardless, the cells are expected to stimulate growth and functional improvement via release of soluble signals, production of extracellular matrix (ECM), and/or differentiation and incorporation into new tissues. 2) Cell-free approaches where biomaterials are implanted and induce cell recruitment, proliferation, or healing either directly or through the release of therapeutic factors. 3) Combined techniques where cells and biomaterials are organized in a defined way and then implanted as a single unit. 4) Bioreactor-based approaches where tissue formation is initiated and optimized in controlled *in vitro* settings prior to implantation in the body.

Generic imaging needs can be identified that are applicable to one or more of the approaches. For techniques involving biomaterials, the ability to quantitatively evaluate the 3D structure of scaffolds used is important prior to application, in bioreactors and within tissue. While imaging materials for characterization prior to application is relatively well-developed, it is often difficult to visualize the 3D structure of a degradable scaffold as it interacts with cells and tissue in TERM applications. For methods based on cell delivery, it may be important to track the location, differentiation and function of these cells within the engineered tissues and potentially in ectopic regions. Both tracking of cells and biomaterials is important, but the ultimate imaging goal of any application is examination of the structure and function of the tissue response generated following application of these therapies. There are several imaging modalities that have been investigated for specific TERM applications. This review will focus on available imaging modalities summarizing how they have been employed to address imaging challenges in TERM as well as discussing their limitations and potential for further development.

1.2. Imaging modalities

All forms of imaging require interactions of electromagnetic or mechanical energy with an object. Images are generated by measuring changes in the energy due to absorption, refraction, or scatter resulting from these interactions. The imaging depth, contrast, and spatial resolution achieved by a given imaging modality are largely based on the type and frequency of energy employed. Imaging depths range from less than a hundred microns to the entire body, while spatial resolution ranges from submicron to a few millimeters (Fig. 2B). This review will focus on six wavelength, or equivalently, frequency, ranges of electromagnetic or acoustic radiation and the imaging modalities that use them, namely: Ultrasound (US), Photoacoustic Microscopy (PAM), Magnetic Resonance Imaging (MRI), Optical Imaging, X-ray Imaging, and Nuclear Imaging.

2. Ultrasound

Conventional ultrasound (US) imaging (1–50 MHz) utilizes acoustic waves produced by a transducer that travel through the medium to a specific focusing depth. The transducer not only generates energy but also acts as a receiver of the returning signal. Contrast results from differences in ultrasonic reflectivity, and an image is generated based on the time required for the wave to echo back as well as the strength of the signal received. This process can be repeated at several depths in order to produce a 3D map of the object. Various US imaging schemes have been applied to assess biomaterials, engineered tissue constructs, cells, and newly formed tissue.

Clinically, US has been used for decades to image flow in blood vessels. Similarly, it has been applied for the evaluation of patency and flow in tissue engineered vascular grafts *in vitro* and *in vivo* [2–6] (Fig. 3A). In many TERM applications, it is important to go beyond assessment of large vessel function and evaluate the structure of microvascular networks within tissue [7]. This structure is essential to proper tissue function. Intravascular injection of microbubbles can enhance US contrast, allowing imaging of small vessels typically invisible in US [8]. Power doppler US imaging has been applied to detect vessels 100–150 microns in diameter. While not capable of directly imaging microvessels smaller than 100 microns, regions of increased vascularization can be identified based on aggregate signals resulting from microbubbles present in multiple small vessels [9]. Recently, US with microbubbles has been applied toward the assessment of vascularization of hydrogels *in vivo* [10].

US imaging has been applied directly to the evaluation of engineered tissues and biomaterials. Changes in US attenuation possibly resulting from ECM deposition have been used to evaluate the formation of engineered cartilage *in vitro* [11–14], and the distribution of mineralization in collagen hydrogels has also been tracked based on US attenuation [15]. Longitudinal assessment of adipose tissue engineering [16] and ischemic cardiac tissue regeneration [17] has also been performed with US imaging. US can also be applied to map viscoelastic properties of materials and tissues. The technique, known as US elastography, exploits changes in the US speckle pattern following application of a known force to map tissue displacement and estimate viscoelastic properties of the sample [18–20]. US elastography can be used to track degradation of polymer scaffolds *in vitro* (Fig. 3B) and *in vivo* based on changes in compressive moduli as the material degrades [21,22]. While interesting, this method requires the ability to apply a known force to the tissue and measuring the resulting deformation, which is not possible for many tissue locations.

These are some examples in which US imaging has been used to track tissue development, monitor biomaterial degradation, and assess the function and structure of vasculature. However, this imaging modality can be hindered by speckle noise and limited soft tissue contrast. Moreover, there exists a direct tradeoff between imaging depth and spatial resolution. Imaging at lower frequencies (1 MHz) allows deeper penetration into the sample (~3 cm), but reduces spatial resolution to a few hundred microns [23]. While conventional medical US imaging can penetrate much deeper, the resulting spatial resolution no longer provides the details needed for evaluation of TERM applications. Higher frequency sound waves (50 MHz) have a smaller wavelength and thus are capable of reflecting or scattering from smaller structures (20 microns), but are more easily absorbed by tissues limiting the imaging depth to a few millimeters [23].

3. Optical imaging

Optical imaging is a general term used to describe systems that measure the interaction of infrared (300 GHz–430 THz, 700 nm–1 mm), visible (430–790 THz, 380–700 nm), or

ultraviolet light (790 THz–30 PHz, 10–300 nm) with matter. Depending on the imaging system, the techniques measure scatter, absorption, or luminescence of light that is either transmitted through, or reflected out, of the sample. Properties of the light source, both wavelength and intensity, control the depth of penetration and therefore the size of the volume that can be imaged. Optical imaging techniques can have high spatial resolution capable of visualizing cells and subcellular features but are often limited in regards to the volumes/depths that can be imaged.

Optical microscopy is usually characterized as a two-dimensional imaging technique that involves transmission of visible light through a very thin object. The absorbance, scatter, or interference of the light can be detected to provide high resolution contrast of cellular and subcellular structures. While this method is used in nearly every biological laboratory, it is limited for 3D imaging due to contributions of out of focus light from outside the focal plane, which restricts the thickness of the sample that can be imaged. Digital deconvolution methods have been developed that enable extension of these standard transmitted light methods to 3D [24]. This advancement permits imaging of thicker samples, around a couple hundred microns depending on the opacity of the sample, and can be used to image cellular and material structures without the use of exogenous contrast agents.

Even with the most optimized deconvolution algorithms, there are still limits on the thickness of the sample being imaged. Fluorescence imaging has expanded light microscopy enabling extremely high spatial resolution (submicron) and significantly increased imaging depths. Fluorescent labeling techniques enable a broad diversity of imaging, including cellular interactions, tissue function, and overall structure. In some cases fluorescence microscopy can take advantage of naturally occurring fluorophores to monitor cells, engineered tissues, and biomaterials without the requirement of exogenous labels.

Wide-field epifluorescence microscopy is readily available in most wet laboratories, but is limited in volumes imaged even when combined with deconvolution methods. Confocal Microscopy (CM) is a fluorescence imaging technique that utilizes a laser point source to scan the sample and a pinhole to reduce collection of light from outside the focal plane. Samples can be scanned at multiple depths to create a 3D volumetric image. This system allows for deeper imaging with depths up to 350 microns depending on sample properties [25]. Greater imaging depths can be achieved using multiphoton fluorescence microscopy (MFM). In MFM, simultaneous excitation at multiple long wavelengths results in fluorescence. This allows for greater imaging depth, up to one millimeter, while maintaining subcellular spatial resolution [26]. Many TERM studies have taken advantage of the benefits of fluorescence to evaluate strategies in TERM with volume and spatial resolution dependent on the specifics of the microscopy system used.

Fluorescence microscopy is often used to study engineered tissues *in vitro*. Using fluorescent stains, cells can be observed in dense polymeric scaffolds up to 1 mm thick [27] and the structure of vascular networks imaged [28]. Cell viability within 3D scaffolds can be evaluated based on autofluorescence resulting from intracellular NADH [29]. In addition, fluorescent molecules can be used to track tissue function. Voltage sensitive dyes have been used to label cells to optically map arrhythmias within tissue cultures [30]. The natural fluorescent properties of materials can enable imaging of tissue or material structure. Collagen structure can be imaged based on reflectance of visible light at 488 nm [31] and within the 700–1000 nm range using second harmonic generation (SHG) microscopy [32–34]. Collagen crosslinks exhibit fluorescence that can be used to image ECM structure in tissue [35]. Some synthetic polymers also exhibit inherent autofluorescence which can be exploited to image 3D structure (Fig. 4A) and monitor degradation of scaffolds used in tissue engineering applications [36].

These techniques can also be applied for imaging cells and scaffolds *in vivo*. Many different cells have been labeled with fluorescent markers, transplanted, and tracked in small animals [37]. However, the imaged tissue must be near the surface and/or prepared in a special optically transparent window chamber. Hydrogel scaffolds are a particularly difficult imaging challenge due to their high water content. Modification of hydrogels with a fluorescent tag enables monitoring of degradation *in vitro* and *in vivo* in a subcutaneous implant [38]. The ability to separate fluorescence at multiple wavelengths enables simultaneous imaging of multiple cells, tissue structures, and/or materials. Fluorescently labeled cells have been visualized within autofluorescent scaffolds *in vitro* [26] and *in vivo* [39]. MFM and SHG have been combined to allow non-destructive high resolution detection of molecular interactions of cells with ECM, visualization of ECM structure formation [40], and collagen deposition on scaffolds [32]. Additionally, MFM has been used to detect labeled elastin [41] or autofluorescent proteoglycan [34] with simultaneous SHG imaging of collagen allowing a detailed characterization of ECM structure in engineered cartilage. SHG has also been combined with MFM to simultaneously examine ECM production and Mesenchymal stem cell (MSC) differentiation based on the relative expression of natural fluorophores (NADH, lipofuscin, and flavoprotiens) [33]. MFM can be employed for metabolic imaging of cells on a tissue engineering scaffold based on NADH and FAD autofluorescence to estimate metabolic activity [42]. A number of sophisticated molecular imaging techniques have been developed and applied for analysis of tumors, including methods that allow quantification of *in vivo* receptor binding potentials [43]. Approaches such as these could provide important insight into TERM applications but have not yet been applied to biomaterial systems. Fluorescence microscopy is mostly effective for *in vitro* imaging of cells, scaffolds, and engineered tissue formation. However, these materials must exhibit fluorescence, either naturally or via the incorporation of labels. CM and MFM have shown some promise for *in vivo* TERM imaging but typically require ectopic models that are close to the surface rather than deep inside the body.

Optical Coherence Tomography (OCT) is an optical method analogous to US imaging but with light waves which allows imaging greater tissue depths. A lens focuses light at a designated depth and the measured echo time delay and magnitude of light is detected. This is compared to the original wave in order to generate a 3D mapping of the optical scattering of the sample. There are several different imaging schemes that can be used depending on the geometry and wavelengths of the beam [44]. OCT can image samples up to 2–3 mm thick but spatial resolution diminishes from 1 to 15 microns as depth increases [25,45].

OCT has been used extensively to image cells, track cell migration, visualize cell location, and examine tissue deposition on tissue engineered scaffolds *in vitro*. Time Domain OCT can be used for noninvasive imaging of the porous structure of polymer foams seeded with cell aggregates (Fig. 4B). Using this method, pores in the polymer were initially clearly identified, but as cells proliferated and produced ECM the pores were no longer visible and imaging depth was reduced [46]. OCT has also been utilized to image changes in optical attenuation of cells cultured in agarose gels [47]. Whole-field OCT has been used to observe cell morphology in *in vitro* engineered bone tissue [46]. In this case, cells were labeled with magnetic beads in order to increase visibility [46]. OCT has been used to study cell distribution and migration within polymer scaffolds [48,49] and to examine cell–material interactions [27,48,50]. OCT can be combined with fluorescence imaging techniques to enhance cell visibility within scaffolds [48,50,51]. This approach has enabled the study of cell morphology as a function of feature size of the scaffold structures [50,51].

OCT has proven to be a useful tool for monitoring engineered tissues in bioreactors. Doppler OCT allowed for simultaneous imaging of perfusion and tissue architecture in a tissue engineered artery [52,53]. It can also be used to map local fluid flow and shear stress within

a porous construct [54]. The addition of gold nanoparticles to the perfusion fluid in a bioreactor enhances OCT contrast and allows greater detail into flow dynamics [44]. OCT was also used to longitudinally characterize microchannel scaffolds seeded with cells [55,56]. Different culture conditions were compared and assessed for cell density and ECM deposition determined by OCT. Porous structure was easily identified until the channels were populated completely by cells [55]. Collagen gels seeded with tenocytes were also imaged with OCT in order to observe fiber arrangement and development in a flow chamber [57].

Polymer scaffolds exhibit contrast in OCT that has been used to track structure *in vitro* and *in vivo*. Changes in construct architecture of both acellular dermis and cell seeded collagen gels have been imaged with OCT for engineered skin applications [44,58,59]. OCT has also been applied for *in vivo* imaging of hydrogels for wound healing applications [39] as well as following injection into the vitreous of the eye [60]. Recently, Optical Coherence Elastography (OCE) has been examined for the characterization of biomaterials [61]. Similar to US Elastography, OCE maps the elastic modulus of a sample based on changes in optical scattering following an applied stress [61]. This technique can be used to monitor changes in stiffness of engineered tissues resulting from cell proliferation and increased production of ECM [48,62].

Bioluminescent Imaging (BLI) is a technique that detects light emitted from biological samples. BLI requires the introduction of luciferase into either the animal or cells (Fig. 4C). In many studies BLI is used to track cells following implantation. Luciferase transfection of MSCs allowed identification of cell location following injection [63,64]. Stem cell viability, proliferation, and migration on various polymer scaffolds have been monitored noninvasively for months using BLI [65–67]. BLI was also employed to monitor stem cell proliferation on polymer scaffolds in a bioreactor [66]. Bone tissue engineering strategies have used mice genetically modified to express luciferase during bone formation [63,64], as well as luciferase transfected stem cells [68–70] to examine tissue engineered bone. Exploitation of tissue-specific luciferase reporters can be used to examine MSC differentiation in tissue engineering environments [71]. BLI allows for noninvasive, longitudinal imaging of cells and engineered tissue *in vivo* and, depending on the promoter used, can provide functional information. However, the technique requires the introduction of a luciferase gene and does not give three-dimensional spatial information.

Applying multiple optical imaging techniques to the same sample can produce both structural and functional information. Prevascularized tissue constructs implanted in dorsal window chambers of immunodeficient mice were monitored for two weeks using intravital microscopy, multispectral imaging, and laser speckle imaging. These three techniques combine to provide images of vessel morphology, blood flow, and hemoglobin oxygen saturation. The flow maps showed that perfusion did not persist due to thrombi formation, a result that could not be seen in the structural images alone [72]. Using optical techniques to map function proved to be a novel way to identify a failure mechanism of the tissue engineered construct.

Optical imaging techniques have been widely used in TERM applications but still have limitations primarily in regards to imaging depth. Some newer systems have been developed to try to overcome this limitation. A technique based on laminar optical tomography has been used to image thicker collagen scaffolds (3 mm) seeded with cells labeled with a fluorescent maker [73]. Bioreactor systems have been imaged by incorporation of micro-imaging channels with fiber optics into biomaterials. Fluorescently labeled cells could then be seen through a 3 mm thick sample [74,75]. While these examples do increase imaging

depth, they are still limited in regards to the volume required for imaging samples within animal models.

4. Photoacoustic microscopy

Photoacoustic microscopy (PAM) is a rapidly emerging hybrid modality that combines optical image contrast with US detection principles [76]. The goal of PAM is to estimate an object's spatially variant absorbed optical energy density from measurements of pressure wavefields that are induced via the photoacoustic effect. Because the optical absorption characteristics of tissue vary strongly with hemoglobin content, knowledge of the absorbed optical energy distribution can yield both structural and functional information.

In PAM, short pulses of near infrared energy are delivered to an object. The optical energy is absorbed rapidly and converted to heat, which creates sound waves that can be detected by a US transducer [77]. Large tissue image contrast is created by differences in optical absorption. However, because US waves are the detected signal, PAM overcomes some of the imaging depth limitations of pure optical techniques. Due to these advantages, PAM has shown promise for imaging in TERM applications.

PAM has been successfully used to resolve vasculature in rodents brains [78] and angiogenesis in tumors [79–81] *in vivo*. Since, oxyhemoglobin is a strong absorber of light at certain wavelengths (570 nm, 900 nm, 1064 nm), scanning at those wavelengths allows imaging of oxygenated blood and therefore functional blood vessels. Neovascularization into porous polymer foams implanted in mice ears was monitored over a six-week time period using PAM, with capillary level resolution [82] (Fig. 5A). Contrast agents, especially gold particles, can be introduced to enhance image contrast in PAM [77] and have been used to help visualize cells and vasculature. Targeting gold nanoparticles to specific tissues allows the use of spectroscopic PAM for simultaneous imaging of vasculature and tissue structure. Imaging at various wavelengths allowed separate mapping of blood oxygen saturation and nanoparticle distribution [83]. Gold nanoparticles have also been targeted to endothelial cells to enhance visualization of angiogenesis with PAM as demonstrated *in vivo* in a hydrogel scaffold containing FGF-2 [84]. PAM can also be used for monitoring cells seeded on porous polymer scaffolds and cultured *in vitro* in order to compare cellular distribution and tissue formation between different culture conditions [85].

PAM can be used in conjunction with US imaging to acquire separate volumes of different image contrasts. Stem cells labeled with gold nanotracers and suspended in hydrogels were monitored both *in vitro* [86,87] and *in vivo* [87] using this approach. Relatively low concentrations of cells could be detected (down to 1×10^4 cells/mL) [87]. The multimodal US/PAM system could identify hydrogel boarders and volume change *in vitro* [86] (Fig. 5B); however, this could not be achieved *in vivo* [87]. US/PAM system has also used to monitor vascular ingrowth into explanted MSC seeded hydrogels [88].

PAM addresses a number of shortcomings of US and optical imaging methods and shows significant potential for tracking cells and monitoring engineered tissues. However, longitudinal studies may be difficult since signals are dependent on local laser fluence which changes with tissue growth and repositioning of samples/animals between imaging sessions. Also, while PAM shows improvements over the depth and resolution issues of US and optical methods, for TERM applications PAM is still limited in regards to tissue penetration as maximum depth is on the level of several millimeters.

5. Magnetic resonance imaging

Image contrast in magnetic resonance imaging (MRI) is typically related to differences in the proton density in a sample. A large magnetic field, ranging from 1.5 to 11.7 T, is applied to the sample aligning the majority of the nuclei in the direction of the field. Radiofrequency pulses are applied to alter the magnetization systematically generating rotating magnetic fields that can be measured. Protons in different materials and conditions realign at different rates generating image contrast. Many pulse frequency patterns can be applied to create images based on different contrast mechanisms including T1 and T2 relaxation times, diffusion weighted, proton density, and magnetic transfer ratio (MTR). Using these different schemes, MRI can provide both anatomical and functional information [89].

MRI possesses excellent soft tissue contrast allowing for soft tissue segmentation and volume quantification making it very valuable for TERM applications. Adipose can be easily identified from other tissues using T1 weighted images [90,91], and this has been exploited for monitoring of the development of engineered adipose tissue [92,93]. MRI has also been used to differentiate between newly formed bone, adipose, and residual scaffold in a tissue engineered phalange model based on the combination of multiple contrast mechanisms [94] (Fig. 6A). MRI has been successful in imaging changes in bioprosthetic heart valves prior to failure [95] which is important in predicting the life expectancy of the implant.

Contrast enhancement can be used to further expand the capabilities of MRI. The most popular contrast agents for TERM applications are Super Paramagnetic Iron Oxide Nanoparticles (SPIONs). SPIONs produce regions of low intensity in MRI images. It is relatively straightforward to label cells with SPIONs, which enables visualizing and tracking both *in vitro* on scaffolds and *in vivo* with MRI. A wide variety of cells have been successfully labeled with SPIONs including MSCs, neural stem cells, human adipose-derived stromal cells (ASCs), chondrocytes, macrophages, and smooth muscle cells [64,89,96–107].

SPION labeling has been combined with MRI to study cell distribution in polymer scaffolds (Fig. 6B) [96,102,104,106,108,109] and to noninvasively monitor their presence in engineered tissues *in vitro* [98,103]. MRI has also been used to track localization of SPION labeled cells to damaged tissues [64,97,105] or areas of inflammation [107] following intravascular injection in small animal models. SPION labeled cells seeded in polymer systems and implanted *in vivo* have been imaged with MRI to determine if the cells are maintained in the target location [64,96,99–102,104]. These investigations demonstrate the successful labeling of cells to increase contrast in MRI images. However, it still remains to be demonstrated conclusively that the incorporation of the iron oxide nanoparticles does not alter cell behavior. Labeling and tracking of cells have not been the only use for SPIONs as a contrast agent for MRI. In one application, SPIONs were functionalized to bind to specific macromolecules within degradable hydrogels. This enabled imaging of the hydrogels following subcutaneous implantation in order to monitor material degradation [110].

MRI has been used as a tool to characterize engineered cartilage *in vitro*. Glycosaminoglycan (GAG) content in chondrocyte seeded hydrogels cultured in a bioreactor were monitored using gadolinium enhanced MRI [111–113] while mechanical properties of the samples were mapped using MR elastography [111]. Changes in T2 weighted images have been used to characterize chondrocytes seeded on constructs for engineered cartilage [114–116]. Cartilage is particularly difficult to image *in vivo*. However, MRI can be used to assess the GAG content of cartilage with gadolinium enhanced MRI. In this technique, T1 weighted images are taken before and after injection of $GdDTPA^{2-}$ and

the fixed charge density can be estimated and correlated to GAG content [113,117]. GAG content plays a role in cartilage tissue strength so this technique can provide insight into cartilage function. This method has been used to study native cartilage in both healthy and diseased tissues of human and animals [92,112]. In addition, studies of cartilage regeneration have been quantitatively compared to normal hyaline cartilage using gadolinium enhanced MRI [118] or T2 weighted images (Fig. 6C) [119,120]. MRI has been employed to characterize cell seeded scaffolds *in vivo* for cartilage engineering applications using T1 weighted images [121].

MRI has been applied frequently for functional and molecular imaging of vascularization. MRI can be used to quantify new vessel formation based on changes in total blood volume [122]. Hydroxyapatite scaffolds coated with growth factors were imaged in the groins of rats for three months with dynamic contrast enhanced MRI monitoring changes in vascularity over time [123]. A similar approach MRI has also been used to study vascularization in hydrogels [124–126]. Vascular hyperpermeability is a marker of abnormal vascularization response and can be evaluated in MRI with contrast agents (albumin-GdDTPA) [127]. SPIONs can be covalently bonded to substrates such as anti-VEGF antibodies in order to enhance detection of angiogenesis with MRI [128,129].

MR microscopy has been employed to generate high resolution (5–10 μm) images of engineered tissues and biomaterials. Changes in collagen and mineral content in an osteoblast-seeded bioreactor could be detected using different contrast schemes. In proton density images, the lowest signal indicated highest mineralization and in MTR images, high signal signified areas of high collagen content [130]. The structure of hydrogel microcapsules has been quantified and tracked over a month in culture using MRI [131]. MR elastography was used to quantify the difference in stiffness between hydrogel seeded with MSCs cultured for osteogenic and adipogenic differentiation both in vitro and *in vivo* [132]. Recently, collagen fiber orientation of arteries has been mapped using diffusion tensor imaging (Fig. 6D). This is similar to data that can be extracted using SHG imaging [133]. However, MRI can be used to image greater depths and much larger volumes.

MRI has been employed extensively to image biomaterials and engineered tissues. It has the capabilities of tracking cells both *in vitro* on tissue engineered constructs and *in vivo* using contrast agents. ECM deposition and mineralization in bioreactors can be visualized and quantified as well as biomaterial architecture. Many different engineered tissues have been monitored for anatomical structure and vascularity. While the contrast agents used are non-toxic, conformation on proper cell/tissue differentiation/function in the presence of these agents is still needed. Determination of safety is vital to any future clinical use of these contrast agents. In addition, while imaging depth is high with MRI, spatial resolution is on the order of hundreds of microns. Better scanners are under development but, typically, spatial resolution is inversely proportional to the field of view. Higher resolution requires scan times of several hours, which can become problematic for *in vivo* imaging.

6. X-ray imaging

X-ray imaging exploits variations in the X-ray absorption, refraction, and/or scattering properties of an object to form image contrast. Most diagnostic X-ray imaging methods utilize higher energy photons (>15 KeV) that have the capability to penetrate through the entire body. Imaging in computed tomography (CT) mode allows for creation of 3D images of the sample. Spatial resolution of X-ray imaging is a function of spot size of the X-ray tube source, or more generally the X-ray beam coherence properties, and the detector properties, but nanometer scale resolution has been achieved [134].

MicroCT (μCT) has been used to image the internal structure of a wide variety of tissue engineering scaffolds prior to use. This technique allows for the non-destructive quantification of scaffold porosity, average pore size, interconnectivity, and other features that are important to control for TERM applications [135–149]. Repeated scanning at different time points permits visualization of how these features of constructs change following degradation *in vitro* [150–153]. Since X-ray absorption-based contrast between soft tissues and biomaterials can be very low, imaging is often performed on freeze-dried samples or under dry conditions rather than under standard culture conditions.

Characterization of tissue engineered bone is the most popular use of μCT due to the highly absorbing properties of mineralized tissues. Repeated scans of cell seeded constructs in culture conditions allow quantification of spatial distributions of mineralization over time [154,155] and within hydrogels [156]. Differences in mineralization due to scaffold thickness and culture conditions (static vs. perfusion) can be quantified from μCT scans at different time points [157]. μCT allows for noninvasive, non-destructive comparison of mineralization based on *in vitro* culture conditions.

X-ray-based imaging has also been used extensively to monitor and study *in vivo* bone tissue engineering using many different biomaterials and animal models. Some studies involve mCT imaging of explanted samples, allowing the segmentation of scaffold, old bone, and newly formed tissue [94,158–161], while others only imaged the newly formed bone [162–164]. *Ex vivo* imaging has been used to analyze osteointegration of implants in bone [165,166]. Multiple longitudinal *in vivo* μCT studies have been performed to monitor bone formation in implanted scaffolds and to compare conditions of growth factor and cell incorporation [123,166–169] (Fig. 7A). Some methods are able to separate scaffold from newly formed bone using μCT but this depends on the biomaterial used and is particularly challenging with bioceramics [170].

In addition to visualizing tissue engineered bone, researchers have sought to characterize neovascularization within engineered tissues. This can be achieved using μCT enhanced with contrast agents such as Microfil or barium sulfate [171–173]. Microfil is a radiodense cast that polymerizes within vessels to display the 3D vascular structure but requires post mortem evaluation. Many studies image samples before and after decalcification in order to gain knowledge on both the newly formed bone (prior to decalcification) and blood vessels (with contrast and after decalcification) [174–176]. Using a synchrotron source for radiation permits the segmentation of bone and microfilled vessels without the decalcification [170]. μCT has also been utilized to evaluate integration of blood vessels and neural tissue in polymeric scaffolds [177].

Contrast agents have been developed to enable μCT imaging of engineered soft tissues. Staining collagen with heavy metal contrast agents displays 3D structure of scaffolds [178,179]. However, the contrast agents can often be toxic, rendering those scaffolds no longer usable. Using high resolution μCT (1.65 microns) stem cells labeled with magnetic nanoparticles could be identified within skeletal muscle after an intra-arterial transplant [180]. Cells seeded on porous scaffolds can also been identified following osmium tetroxide staining and drying allowing study of cell location and distribution [181]. Synchrotron-based μCT has been implemented to visualize individual cartilage cells on porous scaffolds by staining with Au/Ag [182]. μCT has also been employed to monitor a tissue engineering scaffold implanted in the abdomen of rats for six months [183]. Finally, cartilage can be imaged by detecting proteoglycan (PG) content based on the equilibrium partitioning of an ionic contrast agent (Hexabrix 320) via μCT (EPIC-μCT). This technique has been used to monitor ECM within hydrogels containing chondrocytes [174], examine PG content and

distribution in an *in vitro* model of cartilage degradation (Fig. 7B), and for 3D analysis of articular cartilage *in situ* on a rabbit femur [184].

Outside of imaging mineralized tissues, most applications of conventional absorption-based μCT applied to TERM require exogenous contrast agents or drying of samples making it not effective for wide use *in vitro* or *in vivo*. Techniques based on X-ray Phase Contrast (PC) allow imaging based on endogenous X-ray refraction and scatter contrast, which can be up to one thousand times more sensitive than X-ray absorption contrast [185,186]. X-ray PC techniques have recently been investigated for imaging a variety of biomaterials and engineered tissues. X-ray PC techniques have been used to examine the 3D porous structure of dried biomaterials [187–189]. More importantly, X-ray PC has recently been shown to enable imaging of polymer scaffold structure in culture and embedded within tissue [190,191].

X-ray PC imaging has also been implemented to visualize cell and ECM deposition on scaffolds *in vitro*. Gold-lectin stained cells cultured on PET multifilament yarns could be imaged in hydrated conditions. Visualization of the cells resulted from absorption contrast while PC allowed imaging of scaffold structure [192,193]. PGA/PLLA scaffolds seeded with iron oxide nanoparticle labeled cells deposited ECM could be observed in PC X-ray CT scans [194]. Brain tissue embedded within alginate hydrogels could easily be seen with X-ray PC [195] while individual chondrocytes could be identified with an in-line holography imaging scheme in the absence of cell labeling (Fig. 7C) [196,197]. Additionally, X-ray PC imaging has been implemented to visualize immature bone matrix deposited on ceramics scaffolds from osteoblasts and pre-osteoblasts cultured *in vitro* [198].

X-ray PC imaging has seen success in assessing engineered tissue samples *ex vivo* allowing for a more accurate segmentation of scaffolds from newly formed bone and soft tissue ingrowth in engineered tissues [170,190,199–202]. X-ray PC allows improved visualization of the integration of titanium implants with bone over μCT [203]. X-ray PC imaging has also been implemented to enhance bone imaging due to enhanced detail in the architecture of trabecular bone. Differences in the structure and porosity of bone can be detected [204,205] making X-ray PC imaging a means to noninvasively monitor bone remodeling [206].

The primary advantage of X-ray PC is enhanced soft tissue and biomaterial contrast without the use of exogenous contrast agents. X-ray PC techniques have shown promise for imaging cartilage [207] and vasculature [186,208,209] without using contrast agents. Vascular networks within explanted ceramic scaffolds could be seen in propagation-based X-ray images allowing quantification of vessel properties [210]. Hydrogels that are invisible in traditional absorption-based X-ray imaging can be identified *in vitro* and in tissue using X-ray PC techniques (Fig. 7D) [211].

X-ray imaging, both absorption and PC, has been applied for evaluation of biomaterials and engineered tissue *in vitro* and *in vivo*. These techniques are capable of high resolution, high contrast, 3D volume renderings of large samples and structures deep within the body. However, these modalities require use of ionizing radiation, so energy and scan time need to be optimized in order to prevent tissue or sample damage. A current limitation to X-ray PC imaging is the relatively long data-acquisition times that are required when implemented with a benchtop X-ray source. Reducing data-acquisition times remains an active area of research and is likely to lead to imaging of TERM application *in vivo* [212,213].

7. Nuclear imaging

Nuclear Imaging is based on techniques that detect gamma rays emitted from radioactive substances. Radiopharmaceuticals are introduced into the body or tissue and areas of high uptake are detected as they decay and emit radiation. Specific radiotracers can be used to identify targeted activity. This technique has been useful in the diagnosis of disease including many cancers and hyperthyroidism as well as in detecting localized inflammation through the mapping of leukocyte distribution [64]. The two most common 3D forms of nuclear medicine are Positron Emission Tomography (PET) and Single Positron Emission Computed Tomography (SPECT). Both are capable of relaying functional information about tissue but not anatomical data. Therefore, they can be combined with MRI or CT to create a combined picture of structure and function. Small animal hybrid MR–PET systems are being developed and could be used for monitoring tissue engineering performance [89].

Nuclear imaging techniques have been applied to detect activity in engineered tissues in a number of settings [214]. In laboratory studies, PET has been used to detect the glycolic activity of multiple cell types using ^{18}FDG, which allows acquisition of data from extremely low concentrations of cells [215,216]. This same radiotracer has been used to compare cell viability of cardiomyocytes embedded in fibrin in both a pulsatile flow chamber and static culture, identifying enhanced metabolic activity in the perfused chambers [217]. Cell adherence and viability of progenitor cells on decellularized tissues was characterized with this radiotracer in a bioreactor [218]. In a tracheal tissue engineering model, ^{18}FDG was used to assess function of multiple cells cultured on a synthetic scaffold [219].

PET and SPECT imaging have also been applied to monitor engineered tissues *in vivo* [64,220]. Radiolabeled growth factor delivered from scaffolds can be quantified noninvasively in engineered tissues. When combined with μCT images, the PET data can be used to spatially evaluate growth factor distribution relative to new bone formation [221]. Bone formation in cell seeded ceramic scaffolds implanted in large bone defects in rabbits was tracked with SPECT over a three-month time course (Fig. 8A) [222]. Vascularization within the bioceramics was observed with ^{99}Tc-MDP SPECT over two months [223,224].

Both PET and SPECT have been implemented to track transplanted labeled cells *in vivo* by detecting their metabolic activity. Small animal PET has been successful for tracking transplanted progenitor cells and MSCs for up to seven days [64]. Retention and location of stem cells injected into an ischemic myocardium have been quantified with PET (Fig. 8B) [225] and SPECT [226]. The fate of ASCs seeded on scaffolds for bone defect repair was tracked with SPECT/CT [227]. While these modalities have shown promise for visualizing tissue and cell function, they do not provide any structural information. For this information they need to be implemented with other imaging modalities. Further, they are limited by poor spatial resolution and the need for long scan times [228]. Finally, there can be a non-specific uptake of radiotracers by surrounding normal tissue so it may be difficult to distinguish signal between existing and newly formed tissue [64].

8. Conclusions

The ability to monitor and assess TERM therapies is a critical need. The imaging techniques described here have all been successfully applied to evaluate specific aspects of TERM strategies. However, the ideal technique depends on specifics of the application and research. Optical imaging and PAM/US appear better suited for *in vitro* monitoring with potential for certain *in vivo* studies. MRI, X-ray, and nuclear imaging show more promise for *in vivo* applications due to the spatial resolution and imaging depth capabilities for each system. As advances in each modality are made to improve these capabilities, their

applications toward the characterization of structure and function of scaffolds and engineered tissues will expand. In addition, advances in contrast agents and imaging strategies should be developed specifically for TERM applications. In many cases, the application of multiple imaging modalities is likely to improve analysis as it does currently for many clinical applications. The strengths of each system can be exploited in order to give a comprehensive picture of changes occurring to both structure and function during the tissue engineering process. It is imperative that researchers continue to investigate and optimize these imaging modalities as assessment tools and move away from traditional two-dimensional methods so the transition to the clinical setting can be efficient and accelerated.

Acknowledgments

Research described here has been supported in part by the Veterans Administration, the National Science Foundation (DIIS 1125412 and CBET 0854430), and the National Institute of Health (R01EB009715). The authors would like to thank Dr. Bin Jiang, Dr. Lihong Wang, and Dr. Laura Suggs for providing images for the figures.

References

[1]. Multi-agency tissue engineering science: a foundation for the future. Advancing tissue science and engineering: a multi-agency strategic plan. Jun. 2007

[2]. Assmann A, Akhyari P, Delfs C, Flogel U, Jacoby C, Kamiya H, et al. Development of a growing rat model for the in vivo assessment of engineered aortic conduits. J Surg Res. 2012; 176:367–75. [PubMed: 22172135]

[3]. Hibino N, Duncan DR, Nalbandian A, Yi T, Qyang Y, Shinoka T, et al. Evaluation of the use of an IPS cell sheet for the construction of tissue engineered vascular grafts. J Thorac Cardiovasc Surg. 2012; 143:696–703. [PubMed: 22244569]

[4]. Matsumura G, Nitta N, Matsuda S, Sakamoto Y, Isayama N, Yamazaki K, et al. Long-term results of cell-free biodegradable scaffolds for in situ tissue-engineering vasculature: in a canine inferior vena cava model. PloS ONE. 2012; 7

[5]. Quint C, Arief M, Muto A, Dardik A, Niklason LE. Allogeneic human tissue-engineered blood vessel. J Vasc Surg. 2012; 55:790–8. [PubMed: 22056286]

[6]. Tillman BW, Yazdani SK, Neff LP, Corriere MA, Christ GJ, Soker S, et al. Bioengineered vascular access maintains structural integrity in response to arteriovenous flow and repeated needle puncture. J Vasc Surg. 2012; 56:783–93. [PubMed: 22917043]

[7]. Brey EM, King TW, Johnston C, McIntire LV, Reece GP, Patrick CW Jr. A technique for quantitative three-dimensional analysis of microvascular structure. Microvasc Res. 2002; 63:279–94. [PubMed: 11969305]

[8]. Dayton PA, Rychak JJ. Molecular ultrasound imaging using microbubble contrast agents. Front Biosci. 2007; 12:5124–42. [PubMed: 17569635]

[9]. Xuan JW, Bygrave M, Jiang H, Valiyeva F, Dunmore-Buyze J, Holdsworth DW, et al. Functional neoangiogenesis imaging of genetically engineered mouse prostate cancer using three-dimensional power doppler ultrasound. Cancer Res. 2007; 67:2830–9. [PubMed: 17363606]

[10]. Kang K-Y, Allen P, Bischoff J. Bioengineered human vascular networks transplanted into secondary mice reconnect with the host vasculature and re-establish perfusion. Blood. 2011; 118:6718–21. [PubMed: 22039257]

[11]. Fite BZ, Decaris M, Sun Y, Lam A, Ho CK, Leach JK, et al. Noninvasive multimodal evaluation of bioengineered cartilage constructs combining time-resolved fluorescence and ultrasound imaging. Tissue Eng Part C Methods. 2011; 17:495–504. [PubMed: 21303258]

[12]. Kreitz S, Dohman G, Hasken S, Schmitz-Rode T, Mela P, Jockenhoevel S. Nondestructive method to evaluate the collagen content of fibrin-based tissue engineered structures via ultrasound. Tissue Eng Part C Methods. 2011; 17:1021–6. [PubMed: 21663456]

[13]. Rice MA, Waters KR, Anseth KS. Ultrasound monitoring of cartilaginous matrix evolution in degradable peg hydrogels. Acta Biomater. 2009; 5:152–61. [PubMed: 18793879]

[14]. Sun Y, Responte D, Xie H, Liu J, Fatakdawala H, Hu J, et al. Nondestructive evaluation of tissue engineered articular cartilage using time-resolved fluorescence spectroscopy and ultrasound backscatter microscopy. Tissue Eng Part C Methods. 2012; 18:215–26. [PubMed: 22010819]

[15]. Gudur M, Rao RR, Hsaio Y-S, Peterson AW, Deng CX, Stegemann JP. Noninvasive, quantitative, spatiotemporal characterization of mineralization in three-dimensional collagen hydrogels using high-resolution spectral ultrasound imaging. Tissue Eng Part C Methods. 2012; 18:935–45. [PubMed: 22624791]

[16]. Tsuji W, Inamoto T, Ito R, Morimoto N, Tabata Y, Toi M. Simple and longstanding adipose tissue engineering in rabbits. J Artif Organs. 2013; 16:110–4. [PubMed: 23114565]

[17]. Kawamura M, Miyagawa S, Miki K, Saito A, Fukushima S, Higuchi T, et al. Feasibility, safety, and therapeutic efficacy of human induced pluripotent stem cell-derived cardiomyocyte sheets in a porcine ischemic cardiomyopathy model. Circulation. 2012; 126:S29–37. [PubMed: 22965990]

[18]. Jordan P, Socrate S, Zickler TE, Howe RD. Constitutive modeling of porcine liver in indentation using 3D ultrasound imaging. J Mech Behav Biomed Mater. 2009; 2:192–201. [PubMed: 19627823]

[19]. Liu D, Ebbini ES. Viscoelastic property measurement in thin tissue constructs using ultrasound. IEEE Trans Ultrason Ferroelectr Freq Control. 2008; 55:368–83. [PubMed: 18334343]

[20]. Walker JM, Myers AM, Schluchter MD, Goldberg VM, Caplan AI, Berilla JA, et al. Nondestructive evaluation of hydrogel mechanical properties using ultrasound. Ann Biomed Eng. 2011; 39:2521–30. [PubMed: 21773854]

[21]. Kim K, Jeong CG, Hollister SJ. Non-invasive monitoring of tissue scaffold degradation using ultrasound elasticity imaging. Acta Biomater. 2008; 4:783–90. [PubMed: 18348913]

[22]. Yu J, Takanari K, Hong Y, Lee KW, Amoroso NJ, Wang Y, et al. Non-invasive characterization of polyurethane-based tissue constructs in a rat abdominal repair model using high frequency ultrasound elasticity imaging. Biomaterials. 2013; 34:2701–9. [PubMed: 23347836]

[23]. Fouras A, Kitchen MJ, Dubsky S, Lewis RA, Hooper SB, Hourigan K. The past, present, and future of X-ray technology for in vivo imaging of function and form. J Appl Phys. 2009; 105:102009.

[24]. Holmes T, Larson JC, Turturro M, Vaicik M, Papavassilliou G, Larkin S, et al. Multimodality, multispectral and 3D light microscopy of engineered tissues without dyes. J Tissue Eng Regen Med. 2012; 6:1–429.

[25]. Boustany NN, Boppart SA, Backman V. Microscopic imaging and spectroscopy with scattered light. Annu Rev Biomed Eng. 2010; 12:285–314. [PubMed: 20617940]

[26]. Georgakoudi I, Rice WL, Hronik-Tupaj M, Kaplan DL. Optical spectroscopy and imaging for the noninvasive evaluation of engineered tissues. Tissue Eng Part B Rev. 2008; 14:321–39. [PubMed: 18844604]

[27]. Smith LE, Smallwood R, Macneil S. A comparison of imaging methodologies for 3D tissue engineering. Microsc Res Tech. 2010; 73:1123–33. [PubMed: 20981758]

[28]. Rytlewski JA, Geuss LR, Anyaeli C, Lewis EW, Suggs L. Three-dimensional image quantification as a new morphometry method for tissue engineering. Tissue Eng Part C Methods. 2012; 18:507–16. [PubMed: 22224751]

[29]. Dittmar R, Potler E, van Zandvcort M, Ito K. Assessment of cell viability in three-dimensional scaffolds using cellular auto-fluorescence. Tissue Eng Part C Methods. 2012; 18:198–204. [PubMed: 21981657]

[30]. Tung L, Zhang Y. Optical imaging of arrhythmias in tissue culture. J Electrocardiol. 2006; 39:S2–6. [PubMed: 17015066]

[31]. Francis-Sedlak ME, Uriel S, Larson JC, Greisler HP, Venerus DC, Brey EM. Characterization of type I collagen gels modified by glycation. Biomaterials. 2009; 30:1851–6. [PubMed: 19111897]

[32]. Rice WL, Firdous S, Gupta S, Hunter M, Foo CW, Wang Y, et al. Non-invasive characterization of structure and morphology of silk fibroin biomaterials using non-linear microscopy. Biomaterials. 2008; 29:2015–24. [PubMed: 18291520]

[33]. Rice WL, Kaplan DL, Georgakoudi I. Two-photon microscopy for noninvasive, quantitative monitoring of stem cell differentiation. PloS ONE. 2010; 5

[34]. Werkmeister E, Dumas D, de Isla N, Marchal L, Stoltz JF. Interest of multimodal imaging in tissue engineering. Biomed Mater Eng. 2008; 18:329–33. [PubMed: 19065043]

[35]. Chiu YC, Cheng MH, Engel H, Kao SW, Larson JC, Gupta S, et al. The role of pore size on vascularization and tissue remodeling in peg hydrogels. Biomaterials. 2011; 32:6045–51. [PubMed: 21663958]

[36]. Chiu YC, Brey EM, Perez-Luna VH. A study of the intrinsic autofluorescence of poly(ethylene glycol)-co-(l-lactic acid) diacrylate. J Fluoresc. 2012; 22:907–13. [PubMed: 22218971]

[37]. Ang LY, Lim ME, Ong LC, Zhang Y. Applications of upconversion nanoparticles in imaging, detection and therapy. Nanomedicine. 2011; 6:1273–88. [PubMed: 21929461]

[38]. Artzi N, Oliva N, Puron C, Shitreet S, Artzi S, bon Ramos A, et al. In vivo and in vitro tracking of erosion in biodegradable materials using non-invasive fluorescence imaging. Nat Mater. 2011; 10:704–9. [PubMed: 21857678]

[39]. Lammers G, Verhaegen PD, Ulrich MM, Schalkwijk J, Middelkoop E, Weiland D, et al. An overview of methods for the in vivo evaluation of tissue-engineered skin constructs. Tissue Eng Part B Rev. 2011; 17:33–55. [PubMed: 21050145]

[40]. Schenke-Layland K, Riemann I, Damour O, Stock UA, Konig K. Two-photon microscopes and in vivo multiphoton tomographs – powerful diagnostic tools for tissue engineering and drug delivery. Adv Drug Deliv Rev. 2006; 58:878–96. [PubMed: 17011064]

[41]. Schenke-Layland K. Non-invasive multiphoton imaging of extracellular matrix structures. J Biophotonics. 2008; 1:451–62. [PubMed: 19343671]

[42]. Ward A, Quinn KP, Bellas E, Georgakoudi I, Kaplan DL. Noninvasive metabolic imaging of engineered 3D human adipose tissue in a perfusion bioreactor. PloS ONE. 2013; 8

[43]. Tichauer KM, Samkoe KS, Sexton KJ, Hextrum SK, Yang HH, Klubben WS, et al. In vivo quantification of tumor receptor binding potential with dual-reporter molecular imaging. Mol Imaging Biol. 2012; 14:584–92. [PubMed: 22203241]

[44]. Matcher SJ. Practical aspects of OCT imaging in tissue engineering. Methods Mol Biol. 2011; 695:261–80. [PubMed: 21042978]

[45]. Fujimoto JG. Optical coherence tomography for ultrahigh resolution in vivo imaging. Nat Biotechnol. 2003; 21:1361–7. [PubMed: 14595364]

[46]. Yang Y, Dubois A, Qin XP, Li J, El Haj A, Wang RK. Investigation of optical coherence tomography as an imaging modality in tissue engineering. Phys Med Biol. 2006; 51:1649–59. [PubMed: 16552095]

[47]. Xu X, Wang RK, El Haj A. Investigation of changes in optical attenuation of bone and neuronal cells in organ culture or three-dimensional constructs in vitro with optical coherence tomography: relevance to cytochrome oxidase monitoring. Eur Biophys J. 2003; 32:355–62. [PubMed: 12851793]

[48]. Liang X, Graf BW, Boppart SA. Imaging engineered tissues using structural and functional optical coherence tomography. J Biophotonics. 2009; 2:643–55. [PubMed: 19672880]

[49]. Zheng K, Rupnick MA, Liu B, Brezinski ME. Three dimensional OCT in the engineering of tissue constructs: a potentially powerful tool for assessing optimal scaffold structure. Open Tissue Eng Regen Med J. 2009; 2:8–13. [PubMed: 19997536]

[50]. Tan W, Oldenburg AL, Norman JJ, Desai TA, Boppart SA. Optical coherence tomography of cell dynamics in three-dimensional tissue models. Opt Express. 2006; 14:7159–71. [PubMed: 19529086]

[51]. Chen C-W, Betz MW, Fisher JP, Paek A, Chen Y. Macroporous hydrogel scaffolds and their characterization by optical coherence tomography. Tissue Eng Part C Methods. 2011; 17:101–12.

[52]. Mason C, Markusen JF, Town MA, Dunnill P, Wang RK. Doppler optical coherence tomography for measuring flow in engineered tissue. Biosens Bioelectron. 2004; 20:414–23. [PubMed: 15494219]

[53]. Mason C, Markusen JF, Town MA, Dunnill P, Wang RK. The potential of optical coherence tomography in the engineering of living tissue. Phys Med Biol. 2004; 49:1097–115. [PubMed: 15128192]

[54]. Jia Y, An L, Wang RK. Doppler optical microangiography improves the quantification of local fluid flow and shear stress within 3-D porous constructs. J Biomed Opt. 2009; 14:050504-1–050504-3. [PubMed: 19895100]

[55]. Bagnaninchi PO, Yang Y, Zghoul N, Maffulli N, Wang RK, Haj AJ. Chitosan microchannel scaffolds for tendon tissue engineering characterized using optical coherence tomography. Tissue Eng. 2007; 13:323–31. [PubMed: 17518566]

[56]. Liu MJJ, Chou SM, Chua CK, Tay BCM, Ng BK. The development of silk fibroin scaffolds using an indirect rapid prototyping approach: morphological analysis and cell growth monitoring by spectral-domain optical coherence tomography. Med Eng Phys. 2013; 35:253–62. [PubMed: 22055004]

[57]. Ahearne M, Bagnaninchi PO, Yang Y, El Haj A. Online monitoring of collagen fibre alignment in tissue-engineered tendon by PSOCT. J Tissue Eng Regen Med. 2008; 2:521–4. [PubMed: 18956413]

[58]. Smith LE, Bonesi M, Smallwood R, Matcher SJ, MacNeil S. Using swept-source optical coherence tomography to monitor the formation of neo-epidermis in tissue-engineered skin. J Tissue Eng Regen Med. 2010; 4:652–8. [PubMed: 20603865]

[59]. Wang Z, Pan H, Yuan Z, Liu J, Chen W, Pan Y. Assessment of dermal wound repair after collagen implantation with optical coherence tomography. Tissue Eng Part C Methods. 2008; 14:35–45. [PubMed: 18454644]

[60]. Turturro SB, Guthrie MJ, Appel AA, Drapala PW, Brey EM, Perez-Luna VH, et al. The effects of cross-linked thermo-responsive PNIPAAm-based hydrogel injection on retinal function. Biomaterials. 2011; 32:3620–6. [PubMed: 21320724]

[61]. Sun C, Standish B, Yang VX. Optical coherence elastography: current status and future applications. J Biomed Opt. 2011; 16:043001. [PubMed: 21529067]

[62]. Ko H-J, Tan W, Stack R, Boppart SA. Optical coherence elastography of engineered and developing tissue. Tissue Eng. 2006; 12:63–73. [PubMed: 16499443]

[63]. De Boer J, van Blitterswijk C, Lowik C. Bioluminescent imaging: emerging technology for non-invasive imaging of bone tissue engineering. Biomaterials. 2006; 27:1851–8. [PubMed: 16242768]

[64]. Villa C, Erratico S, Razini P, Farini A, Meregalli M, Belicchi M, et al. In vivo tracking of stem cell by nanotechnologies: future prospects for mouse to human translation. Tissue Eng Part B Rev. 2011; 17:1–11. [PubMed: 20846051]

[65]. Hwang do W, Jang SJ, Kim YH, Kim HJ, Shim IK, Jeong JM, et al. Real-time in vivo monitoring of viable stem cells implanted on biocompatible scaffolds. Eur J Nucl Med Mol Imaging. 2008; 35:1887–98. [PubMed: 18437378]

[66]. Logeart-Avramoglou D, Oudina K, Bourguignon M, Delpierre L, Nicola M-A, Bensidhoum M, et al. In vitro and in vivo bioluminescent quantification of viable stem cells in engineered constructs. Tissue Eng Part C Methods. 2010; 16:447–58. [PubMed: 19624260]

[67]. Roman I, Vilalta M, Rodriguez J, Matthies AM, Srouji S, Livne E, et al. Analysis of progenitor cell-scaffold combinations by in vivo non-invasive photonic imaging. Biomaterials. 2007; 28:2718–28. [PubMed: 17346789]

[68]. Geuze RE, Prins H-J, Oner FC, van der Helm YJM, Schujiff LS, Martens AC, et al. Luciferase labeling for multipotent stromal cell tracking in spinal fusion versus ectopic bone tissue engineering in mice and rats. Tissue Eng Part A. 2010; 16:3343–51. [PubMed: 20575656]

[69]. Olivo C, Alblas J, Verweij V, Van Zonneveld A-J, Dhert WJ, Martens AC. In vivo bioluminescence imaging study to monitor ectopic bone formation by luciferase gene marked mesenchymal stem cells. J Orthop Res. 2008; 26:901–9. [PubMed: 18271011]

[70]. Prins H-J, Fernandes H, Rozemuller H, Van Blitterswijk C, De Boer J, Martens AC. Spatial distribution and survival of human and goat mesenchymal stromal cells on hydroxyapatite and b-tricalcium phosphate. J Tissue Eng Regen Med. 2012

[71]. Bago JR, Aguilar E, Alieva M, Soler-Botija C, Vila OF, Claros S, et al. In vivo bioluminescence imaging of cell differentiation in biomaterials: a platform for scaffold development. Tissue Eng Part A. 2013; 19:593–603. [PubMed: 23013334]

[72]. White SM, Hingorani R, Arora RPS, Hughes CCW, George S, Choi B. Longitudinal in vivo imaging to assess blood flow and oxygenation in implantable engineered tissues. Tissue Eng Part C Methods. 2012; 18:697–709. [PubMed: 22435776]

[73]. Zhao L, Lee VK, Yoo SS, Dai G, Intes X. The integration of 3-D cell printing and mesoscopic fluorescence molecular tomography of vascular constructs within thick hydrogel scaffolds. Biomaterials. 2012; 33:5325–32. [PubMed: 22531221]

[74]. Hofmann MC, Whited BM, Goldstein AS, Freeman JW, Rylander MN, Rylander C, et al. Non-destructive real-time imaging of cell morphology for tissue-engineering applications. IEEE. 2011

[75]. Hofmann MC, Whited BM, Mitchell J, Vogt WC, Criswell T, Rylander C, et al. Scanning-fiber-based imaging method for tissue engineering. J Biomed Opt. 2012; 17:066010-1–066010-11. [PubMed: 22734766]

[76]. Wang LV, Hu S. Photoacoustic tomography: in vivo imaging from organelles to organs. Science. 2012; 335:1458–62. [PubMed: 22442475]

[77]. Su JL, Wang B, Wilson KE, Bayer CL, Chen YS, Kim S, et al. Advances in clinical and biomedical applications of photoacoustic imaging. Expert Opin Med Diagn. 2010; 4:497–510. [PubMed: 21344060]

[78]. Gamelin J, Maurudis A, Aguirre A, Huang F, Guo P, Wang LV, et al. A real-time photoacoustic tomography system for small animals. Opt Express. 2009; 17:10489–98. [PubMed: 19550444]

[79]. Cai X, Li L, Krumholz A, Guo Z, Erpelding TN, Zhang C, et al. Multi-scale molecular photoacoustic tomography of gene expression. PloS ONE. 2012; 7:e43999. [PubMed: 22952846]

[80]. Jose J, Manohar S, Kolkman RG, Steenbergen W, van Leeuwen TG. Imaging of tumor vasculature using Twente photoacoustic systems. J Biophotonics. 2009; 2:701–17. [PubMed: 19718681]

[81]. Siphanto RI, Thumma KK, Kolkman RG, van Leeuwen TG, de Mul FFM, van Neck JW, et al. Serial noninvasive photoacoustic imaging of neovascularization in tumor angiogenesis. Opt Express. 2005; 13:89–95. [PubMed: 19488331]

[82]. Cai X, Zhang Y, Li L, Choi SW, MacEwan MR, Yao J, et al. Investigation of neovascularization in three-dimensional porous scaffolds in vivo by a combination of multiscale photoacoustic microscopy and optical coherence tomography. Tissue Eng Part C Methods. 2013; 19:196–204. [PubMed: 22838500]

[83]. Kim S, Chen YS, Luke GP, Emelianov SY. In vivo three-dimensional spectroscopic photoacoustic imaging for monitoring nanoparticle delivery. Biomed Opt Express. 2011; 2:2540–50. [PubMed: 21991546]

[84]. Pan D, Pramanik M, Senpan A, Allen JS, Zhang H, Wickline SA, et al. Molecular photoacoustic imaging of angiogenesis with integrin-targeted gold nano-beacons. FASEB J. 2011; 25:875–82. [PubMed: 21097518]

[85]. Zhang Y, Cai X, Choi SW, Kim C, Wang LV, Xia Y. Chronic label-free volu-metric photoacoustic microscopy of melanoma cells in three-dimensional porous scaffolds. Biomaterials. 2010; 31:8651–8. [PubMed: 20727581]

[86]. Chung E, Nam SY, Ricles LM, Emelianov S, Suggs L. Evaluation of gold nanotracers to track adipose-derived stem cells in a pegylated fibrin gel for dermal tissue engineering applications. Int J Nanomed. 2013; 8:325–36.

[87]. Nam SY, Ricles LM, Suggs L, Emelianov SY. In vivo ultrasound and photo-acoustic monitoring of mesenchymal stem cells labeled with gold nanotracers. PloS ONE. 2012; 7:e37267. [PubMed: 22615959]

[88]. Nam SY, Mallidi S, Zhang G, Suggs L, Emelianov S. Ultrasound and photoacoustic imaging to monitor vascular growth in tissue engineered constructs. Proc SPIE. 2009; 7179

[89]. Pancrazio JJ, Wang F, Kelley CA. Enabling tools for tissue engineering. Biosens Bioelectron. 2007; 22:2803–11. [PubMed: 17240132]

[90]. Hu HH, Nayak KS, Goran MI. Assessment of abdominal adipose tissue and organ fat content by magnetic resonance imaging. Obes Rev. 2011; 12:e504–15. [PubMed: 21348916]

[91]. Narayan S, Huang F, Johnson D, Gargesha M, Flask CA, Zhang GQ, et al. Fast lipid and water levels by extraction with spatial smoothing (flawless): three-dimensional volume fat/water separation at 7 T. J Magn Reson Imaging. 2011; 33:1464–73. [PubMed: 21591017]

[92]. Xu H, Othman SF, Magin RL. Monitoring tissue engineering using magnetic resonance imaging. J Biosci Bioeng. 2008; 106:515–27. [PubMed: 19134545]

[93]. Xu J, Chen Y, Yue Y, Sun J, Cui L. Reconstruction of epidural fat with engineered adipose tissue from adipose derived stem cells and PLGA in the rabbit dorsal laminectomy model. Biomaterials. 2012; 33:6965–73. [PubMed: 22800536]

[94]. Potter K, Sweet DE, Anderson P, Davis GR, Isogai N, Asamura S, et al. Non-destructive studies of tissue-engineered phalanges by magnetic resonance microscopy and X-ray microtomography. Bone. 2006; 38:350–8. [PubMed: 16256448]

[95]. Smith DB, Sacks MS, Pattany PM, Schroeder R. High-resolution magnetic resonance imaging to characterize the geometry of fatigued porcine bioprosthetic heart valves. J Heart Valve Dis. 1997; 6:424–32. [PubMed: 9263876]

[96]. Andreas K, Georgieva R, Ladwig M, Mueller S, Notter M, Sittinger M, et al. Highly efficient magnetic stem cell labeling with citrate-coated super-paramagnetic iron oxide nanoparticles for MRI tracking. Biomaterials. 2012; 33:4515–25. [PubMed: 22445482]

[97]. Cromer, Berman SM.; Walczak, P.; Bulte, JWM. MRI of transplanted neural stem cells. Magn Reson Neuroimag Method Protocols. 2010; 711:435–49.

[98]. Feng Y, Jin X, Dai G, Liu J, Chen J, Yang L. In vitro targeted magnetic delivery and tracking of superparamagnetic iron oxide particles labeled stem cells for articular cartilage defect repair. J Huazhong Univ Sci Technol Med Sci. 2011; 31:204–9. [PubMed: 21505986]

[99]. Jing X-H, Yang L, Duan X-J, Xie B, Chen W, Li Z, et al. In vivo MR imaging tracking of magnetic iron oxide nanoparticle labeled, engineered, autologous bone marrow mesenchymal stem cells following intra-articular injection. Joint Bone Spine. 2008; 75:432–8. [PubMed: 18448377]

[100]. Lalande C, Miraux S, Derkaoui SM, Mornet S, Bareille R, Fricain JC, et al. Magnetic resonance imaging tracking of human adipose derived stromal cells within three-dimensional scaffolds for bone tissue engineering. Eur Cell Mater. 2011; 21:341–54. [PubMed: 21484704]

[101]. Nelson GN, Roh JD, Mirensky TL, Wang Y, Yi T, Tellides G, et al. Initial evaluation of the use of USPIO cell labeling and noninvasive MR monitoring of human tissue-engineered vascular grafts in vivo. FASEB J. 2008; 22:3888–95. [PubMed: 18711027]

[102]. Poirier-Quinot M, Frasca G, Wilhelm C, Luciani N, Ginefri J-C, Darrasse L, et al. High-resolution 1.5-T magnetic resonance imaging for tissue-engineered constructs: a noninvasive tool to assess three-dimensional scaffold architecture and cell seeding. Tissue Eng Part C Methods. 2012; 16:185–99. [PubMed: 19438301]

[103]. Ramaswamy S, Greco JB, Uluer MC, Zhang Z, Zhang Z, Fishbein KW, et al. Magnetic resonance imaging of chondrocytes labeled with super-paramagnetic iron oxide nanoparticles in tissue-engineered cartilage. Tissue Eng Part A. 2009; 15:3899–910. [PubMed: 19788362]

[104]. Saldanha KJ, Piper SL, Ainslie KM, Desai TA, Kim HT, Majumdar S. Magnetic resonance imaging of iron oxide labelled stem cells: applications to tissue engineering based regeneration of the intervertebral disc. Eur Cell Mater. 2008; 16:17–25. [PubMed: 18677684]

[105]. Sykova E, Jendelova P. Migration, fate and in vivo imaging of adult stem cells in the CNS. Cell Death Differ. 2007; 14:1336–42. [PubMed: 17396130]

[106]. Terrovitis J, Bulte JW, Sarvananthan S, Crowe LA, Sarathchandra P, Batten P, et al. Magnetic resonance imaging of ferumoxide-labeled mesenchymal stem cells seeded on collagen scaffolds — relevance to tissue engineering. Tissue Eng. 2006; 12:2765–75. [PubMed: 17518646]

[107]. Zhang C, Liu T, Gao J, Su Y, Shi C. Recent development and application of magnetic nanoparticles for cell labeling and imaging. Mini Rev Med Chem. 2010; 10:194–203.

[108]. Nitzsche H, Metz H, Lochmann A, Bernstein A, Hause G, Groth T, et al. Characterization of scaffolds for tissue engineering by benchtop-magnetic resonance imaging. Tissue Eng Part C Methods. 2009; 15:513–21. [PubMed: 19191523]

[109]. Heymer A, Haddad D, Weber M, Gbureck U, Jakob PM, Eulert J, et al. Iron oxide labelling of human mesenchymal stem cells in collagen hydrogels for articular cartilage repair. Biomaterials. 2008; 29:1473–83. [PubMed: 18155133]

[110]. Colomb J, Louie K, Massia SP, Bennett KM. Self-degrading, MRI-detectable hydrogel sensors with picomolar target sensitivity. Magn Reson Med. 2010; 64:1792–9. [PubMed: 20648680]

[111]. Neu CP, Arastu HF, Curtiss S, Reddi AH. Characterization of engineered tissue construct mechanical function by magnetic resonance imaging. J Tissue Eng Regen Med. 2009; 3:477–85. [PubMed: 19530259]

[112]. Nugent AE, Reiter DA, Fishbein KW, McBurney DL, Murray T, Bartusik D, et al. Characterization of ex vivo-generated bovine and human cartilage by immunohistochemical, biochemical, and magnetic resonance imaging analyses. Tissue Eng Part A. 2010; 16:2183–96. [PubMed: 20136403]

[113]. Ramaswamy S, Uluer MC, Leen S, Bajaj P, Fishbein KW, Spencer RG. Noninvasive assessment of glycosaminoglycan production in injectable tissue-engineered cartilage constructs using magnetic resonance imaging. Tissue Eng Part C Methods. 2008; 14:243–9. [PubMed: 18620483]

[114]. Irrechukwu ON, Lin P-C, Fritton K, Doty S, Pleshko N, Spencer RG. Magnetic resonance studies of macromolecular contentin engineered cartilage treated with pulsed low-intensity ultrasound. Tissue Eng Part A. 2011; 17:407–15. [PubMed: 20807015]

[115]. Irrechukwu ON, Reiter DA, Lin P-C, Roque RA, Fishbein KW, Spencer RG. Characterization of engineered cartilage constructs using multiexponential T2 relaxation analysis and support vector regression. Tissue Eng Part C Methods. 2012; 18:433–43. [PubMed: 22166112]

[116]. Reiter DA, Irrechukwu ON, Lin P-C, Moghadam S, Von Thaer S, Pleshko N, et al. Improved MR-based characterization of engineered cartilage using multiexponential T2 relaxation and multivariate analysis. NMR Biomed. 2012; 25:476–88. [PubMed: 22287335]

[117]. Freed LE, Guilak F, Guo XE, Gray ML, Tranquillo R, Holmes JW, et al. Advanced tools for tissue engineering: scaffolds, bioreactors, and signaling. Tissue Eng. 2006; 12:3285–305. [PubMed: 17518670]

[118]. Trattnig S, Mamisch TC, Pinker K, Domayer S, Szomolanyi P, Marlovits S, et al. Differentiating normal hyaline cartilage from post-surgical repair tissue using fast gradient echo imaging in delayed gadolinium-enhanced MRI (dGEMRIC) at 3 T. Eur Radiol. 2008; 18:1251–9. [PubMed: 18246356]

[119]. Petersen JP, Ueblacker P, Goepfert C, Adamietz P, Baumbach K, Stork A, et al. Long term results after implantation of tissue engineered cartilage for the treatment of osteochondral lesions in a minipig model. J Mater Sci Mater Med. 2008; 19:2029–38. [PubMed: 17957447]

[120]. Welsch GH, Trattnig S, Hughes T, Quirbach S, Olk A, Blanke M, et al. T2 and T2* mapping in patients after matrix-associated autologous chondrocyte transplantation: initial results on clinical use with 3.0-T MRI. Eur Radiol. 2010; 20:1515–23. [PubMed: 19937329]

[121]. Chou C-H, Lee H-S, Siow TY, Lin M-H, Kumar A, Chang Y-C, et al. Temporal MRI characterization of gelatin/hyaluronic acid/chondroitin sulfate sponge for cartilage tissue engineering. J Biomed Mater Res A. 2012:00A.

[122]. Cheng HL, Loai Y, Farhat WA. Monitoring tissue development in acellular matrix-based regeneration for bladder tissue engineering: multiexponential diffusion and T2* for improved specificity. NMR Biomed. 2012; 25:418–26. [PubMed: 22351641]

[123]. Holt GE, Halpern JL, Lynch CC, Devin CJ, Schwartz HS. Imaging analysis of the in vivo bioreactor: a preliminary study. Clin Orthop Relat Res. 2008; 466:1890–6. [PubMed: 18506563]

[124]. Beaumont M, DuVal MG, Loai Y, Farhat WA, Sandor GK, Cheng HL. Monitoring angiogenesis in soft-tissue engineered constructs for calvarium bone regeneration: an in vivo longitudinal DCE-MRI study. NMR Biomed. 2010; 23:48–55. [PubMed: 19650039]

[125]. Buschmann J, Welti M, Hemmi S, Neueschwander P, Baltes C, Giovanoli P, et al. Three-dimensional co-cultures of osteoblasts and endothelial cells in degrapol foam: histological and high-field magnetic resonance imaging analyses of pre-engineered capillary networks in bone grafts. Tissue Eng Part A. 2011; 17:291–9. [PubMed: 20799888]

[126]. Kim S, Lee JH, Hyun H, Ashitate Y, Park G, Robichaud K, et al. Near-infrared fluorescence imaging for noninvasive trafficking of scaffold degradation. Sci Rep. 2013; 3:1–7.

[127]. Neeman M. Functional and molecular MR imaging of angiogenesis: seeing the target, seeing it work. J Cell Biochem Suppl. 2002; 39:11–7. [PubMed: 12552597]

[128]. Towner RA, Smith N, Asano Y, Doblas S, Saunders D, Silasi-Mansat R, et al. Molecular magnetic resonance imaging approaches used to aid in the understanding of the tissue

regeneration marker met in vivo: implications for tissue engineering. Tissue Eng Part A. 2010; 16:365–71. [PubMed: 19905873]

[129]. Towner RA, Smith N, Asano Y, He T, Doblas S, Saunders D, et al. Molecular magnetic resonance imaging approaches used to aid in the understanding of angiogenesis in vivo: implications for tissue engineering. Tissue Eng Part A. 2010; 16:357–64. [PubMed: 19663584]

[130]. Chesnick IE, Avallone F, Leapman RD, Landis WJ, Eidelman N, Potter K. Evaluation of bioreactor-cultivated bone by magnetic resonance microscopy and FTIR microspectroscopy. Bone. 2007; 40:904–12. [PubMed: 17174620]

[131]. Constantinidis I, Grant SC, Celper S, Gauffin-Holmberg I, Agering K, Oca-Cossio JA, et al. Non-invasive evaluation of alginate/poly-l-lysine/alginate microcapsules by magnetic resonance microscopy. Biomaterials. 2007; 28:2438–45. [PubMed: 17239948]

[132]. Othman SF, Curtis ET, Plautz SA, Pannier AK, Butler SD, Xu H. MR elastography monitoring of tissue-engineered constructs. NMR Biomed. 2012; 25:452–63. [PubMed: 21387443]

[133]. Ghazanfari S, Driessen-Mol A, Strijkers GJ, Kanters FM, Baaijens FP, Bouten CV. A comparative analysis of the collagen architecture in the carotid artery: second harmonic generation versus diffusion tensor imaging. Biochem Biophys Res Commun. 2012; 426:54–8. [PubMed: 22910417]

[134]. Kerckhofs G, Sainz J, Wevers M, Van de Putte T, Schrooten J. Contrast-enhanced nanofocus computed tomography images the cartilage subtissue architecture in three dimensions. Eur Cell Mater. 2013; 25:179–89. [PubMed: 23389752]

[135]. Alberich-Bayarri A, Moratal D, Escobar Ivirico JL, Rodríguez Hernández JC, Valles-Lluch A, Marti-Bonmati L, et al. Microcomputed tomography and microfinite element modeling for evaluating polymer scaffolds architecture and their mechanical properties. J Biomed Mater Res B Appl Biomater. 2009; 91:191–202. [PubMed: 19425071]

[136]. Buttafoco L, Engbers-Buijtenhuijs P, Poot AA, Dijkstra PJ, Vermes I, Feijen J. Physical characterization of vascular grafts cultured in a bioreactor. Biomaterials. 2006; 27:2380–9. [PubMed: 16289328]

[137]. Chimenti I, Rizzitelli G, Gaetani R, Angelini F, Ionta V, Forte E, et al. Human cardiosphere-seeded gelatin and collagen scaffolds as cardiogenic engineered bioconstructs. Biomaterials. 2011; 32:9271–81. [PubMed: 21890193]

[138]. Guda T, Oh S, Appleford MR, Ong JL. Bilayer hydroxyapatite scaffolds for maxillofacial bone tissue engineering. Int J Oral Maxillofac Implants. 2012; 27:288–94. [PubMed: 22442766]

[139]. Ho ST, Hutmacher DW. A comparison of micro CT with other techniques used in the characterization of scaffolds. Biomaterials. 2006; 27:1362–76. [PubMed: 16174523]

[140]. Jones JR, Atwood RC, Poologasundarampillai G, Yue S, Lee PD. Quantifying the 3D macrostructure of tissue scaffolds. J Mater Sci Mater Med. 2009; 20:463–71. [PubMed: 18839281]

[141]. Landis FA, Stephens JS, Cooper JA, Cicerone MT, Lin-Gibson S. Tissue engineering scaffolds based on photocured dimethacrylate polymers for in vitro optical imaging. Biomacromolecules. 2006; 7:1751–7. [PubMed: 16768394]

[142]. Lin A, Barrows TH, Cartmell S, Guldberg R. Microarchitectural and mechanical characterization of oriented porous polymer scaffolds. Biomaterials. 2003; 24:481–9. [PubMed: 12423603]

[143]. Muller B, Beckmann F, Huser M, Maspero F, Szekely G, Ruffieux K, et al. Nondestructive three-dimensional evaluation of a polymer sponge by micro-tomography using synchrotron radiation. Biomol Eng. 2002; 19:73–8. [PubMed: 12202165]

[144]. Oliveira AL, Malafaya PB, Costa SA, Sousa RA, Reis RL. Micro-computed tomography (micro-CT) as a potential tool to assess the effect of dynamic coating routes on the formation of biomimetic apatite layers on 3D-plotted biodegradable polymeric scaffolds. J Mater Sci Mater Med. 2007; 18:211–23. [PubMed: 17323152]

[145]. Voronov R, Vangordon S, Sikavitsas VI, Papavassiliou DV. Computational modeling of flow-induced shear stresses within 3D salt-leached porous scaffolds imaged via micro-CT. J Biomech. 2010; 43:1279–86. [PubMed: 20185132]

[146]. Yan L-P, Oliveira JM, Oliveira AL, Caridade S, Mano JF, Reis RL. Macro/microporous silk fibroin scaffolds with potential for articular cartilage and meniscus tissue engineering applications. Acta Biomater. 2012; 8:289–301. [PubMed: 22019518]

[147]. Yang Y, Dorsey SM, Becker ML, Lin-Gibson S, Schumacher GE, Flaim GM, et al. X-ray imaging optimization of 3D tissue engineering scaffolds via combinatorial fabrication methods. Biomaterials. 2008; 29:1901–11. [PubMed: 18242689]

[148]. Yue S, Lee PD, Poologasundarampillai G, Yao Z, Rockett P, Delvin AH, et al. Synchrotron X-ray microtomography for assessment of bone tissue scaffolds. J Mater Sci Mater Med. 2010; 21:847–53. [PubMed: 19820901]

[149]. Patel ZS, Ueda H, Yamamoto M, Tabata Y, Mikos AG. In vitro and in vivo release of vascular endothelial growth factor from gelatin microparticles and biodegradable composite scaffolds. Pharm Res. 2008; 25:2370–8. [PubMed: 18663411]

[150]. Behravesh E, Timmer MD, Lemoine JJ, Liebschner MA, Mikos AG. Evaluation of the in vitro degradation of macroporous hydrogels using gravimetry, confined compression testing, and microcomputed tomography. Biomacromolecules. 2002; 3:1263–70. [PubMed: 12425664]

[151]. Hedberg EL, Shih CK, Lemoine JJ, Timmer MD, Liebschner MA, Jansen JA, et al. In vitro degradation of porous poly(propylene fumarate)/poly(dl-lactic-co-glycolic acid) composite scaffolds. Biomaterials. 2005; 26:3215–25. [PubMed: 15603816]

[152]. Shi M, Kretlow JD, Nguyen A, Young S, Scott Baggett L, Wong ME, et al. Antibiotic-releasing porous polymethylmethacrylate constructs for osseous space maintenance and infection control. Biomaterials. 2010; 31:4146–56. [PubMed: 20153893]

[153]. Spiller KL, Holloway JL, Gribb ME, Lowman AM. Design of semi-degradable hydrogels based on poly(vinyl alcohol) and poly(lactic-co-glycolic acid) for cartilage tissue engineering. J Tissue Eng Regen Med. 2011; 5:636–47. [PubMed: 21774087]

[154]. Cartmell S, Huynh K, Lin A, Nagaraja S, Guldberg R. Quantitative micro-computed tomography analysis of mineralization within three-dimensional scaffolds in vitro. J Biomed Mater Res A. 2004; 69:97–104. [PubMed: 14999756]

[155]. Sikavitsas VI, Bancroft GN, Lemoine JJ, Liebschner MAK, Dauner M, Mikos AG. Flow perfusion enhances the calcified matrix deposition of marrow stromal cells in biodegradable nonwoven fiber mesh scaffolds. Ann Biomed Eng. 2005; 33:63–70. [PubMed: 15709706]

[156]. Chatterjee K, Lin-Gibson S, Wallace WE, Parekh SH, Lee YJ, Cicerone MT, et al. The effect of 3D hydrogel scaffold modulus on osteoblast differentiation and mineralization revealed by combinatorial screening. Biomaterials. 2010; 31:5051–62. [PubMed: 20378163]

[157]. Porter BD, Lin AS, Peister A, Hutmacher D, Guldberg RE. Noninvasive image analysis of 3D construct mineralization in a perfusion bioreactor. Biomaterials. 2007; 28:2525–33. [PubMed: 17258311]

[158]. Jones AC, Arns CH, Sheppard AP, Hutmacher DW, Milthorpe BK, Knackstedt MA. Assessment of bone ingrowth into porous biomaterials using micro-CT. Biomaterials. 2007; 28:2491–504. [PubMed: 17335896]

[159]. Weiss P, Obadia L, Magne D, Bourges X, Rau C, Weitkamp T, et al. Synchrotron X-ray microtomography (on a micron scale) provides three-dimensional imaging representation of bone ingrowth in calcium phosphate biomaterials. Biomaterials. 2003; 24:4591–601. [PubMed: 12951002]

[160]. Yu H, VandeVord PJ, Mao L, Matthew HW, Wooley PH, Yang SY. Improved tissue-engineered bone regeneration by endothelial cell mediated vascularization. Biomaterials. 2009; 30:508–17. [PubMed: 18973938]

[161]. Zhang Y, Wu C, Friis T, Xiao Y. The osteogenic properties of cap/silk composite scaffolds. Biomaterials. 2010; 31:2848–56. [PubMed: 20071025]

[162]. Hedberg EL, Kroese-Deutman HC, Shih CK, Lemoine JJ, Liebschner MA, Miller MJ, et al. Methods: a comparative analysis of radiography, microcomputed tomography, and histology for bone tissue engineering. Tissue Eng. 2005; 11:1356–67. [PubMed: 16259591]

[163]. Kallai I, Van Lenthe GH, Ruffoni D, Zilberman Y, Muller R, Pelled G, et al. Quantitative, structural and image-based mechanical analysis of nonunion fracture repaired by genetically engineered mesenchymal stem cells. J Biomech. 2010; 43:2315–20. [PubMed: 20471652]

[164]. Kretlow JD, Spicer PP, Jansen JA, Vacanti CA, Kasper FK, Mikos AG. Uncultured marrow mononuclear cells delivered within fibrin glue hydrogels to porous scaffolds enhance bone regeneration within critical-sized rat cranial defects. Tissue Eng Part A. 2010; 16:3555–68. [PubMed: 20715884]

[165]. Bernhardt R, Scharnweber D, Muller B, Thurner P, Schliephake H, Wyss P, et al. Comparison of microfocus-and synchrotron X-ray tomography for the analysis of osteointegration around ti6al4v implants. Eur Cell Mater. 2004; 7:42–51. [PubMed: 15375777]

[166]. Van Lenthe GH, Hagenmuller H, Bohner M, Hollister SJ, Meinel L, Muller R. Nondestructive micro-computed tomography for biological imaging and quantification of scaffold-bone interaction in vivo. Biomaterials. 2007; 28:2479–90. [PubMed: 17258316]

[167]. Leach JK, Kaigler D, Wang Z, Krebsbach PH, Mooney DJ. Coating of VEGF-releasing scaffolds with bioactive glass for angiogenesis and bone regeneration. Biomaterials. 2006; 27:3249–55. [PubMed: 16490250]

[168]. Oest ME, Dupont KM, Kong HJ, Mooney DJ, Guldberg RE. Quantitative assessment of scaffold and growth factor-mediated repair of critically sized bone defects. J Orthop Res. 2007; 25:941–50. [PubMed: 17415756]

[169]. Umoh JU, Sampaio AV, Welch I, Pitelka V, Goldberg HA, Underhill TM, et al. In vivo micro-CT analysis of bone remodeling in a rat calvarial defect model. Phys Med Biol. 2009; 54:2147–61. [PubMed: 19287088]

[170]. Peyrin F. Evaluation of bone scaffolds by micro-CT. Osteoporos Int. 2011; 22:2043–8. [PubMed: 21523402]

[171]. Arkudas A, Beier J, Pryymachuk G, Hoereth T, Bleiziffer O, Polykandriotis E, et al. Automatic quantitative micro-computed tomography evaluation of angiogenesis in an axially vascularized tissue-engineered bone construct. Tissue Eng Part C Methods. 2010; 16:1503–14. [PubMed: 20575690]

[172]. Young S, Kretlow JD, Nguyen C, Bashoura AG, Baggett LS, Jansen JA, et al. Microcomputed tomography characterization of neovascularization in bone tissue engineering applications. Tissue Eng Part B Rev. 2008; 14:295–306. [PubMed: 18657028]

[173]. Zou D, Zhang Z, He J, Zhang K, Ye D, Han W, et al. Blood vessel formation in the tissue-engineered bone with the constitutively active form of HIF-1a mediated BMSCs. Biomaterials. 2012; 33:2097–108. [PubMed: 22172336]

[174]. Guldberg RE, Duvall CL, Peister A, Oest ME, Lin AS, Palmer AW, et al. 3d imaging of tissue integration with porous biomaterials. Biomaterials. 2008; 29:3757–61. [PubMed: 18635260]

[175]. Rai B, Oest ME, Dupont KM, Ho KH, Teoh SH, Guldberg RE. Combination of platelet-rich plasma with polycaprolactone–tricalcium phosphate scaffolds for segmental bone defect repair. J Biomed Mater Res A. 2007; 81:888–99. [PubMed: 17236215]

[176]. Patel ZS, Young S, Tabata Y, Jansen JA, Wong ME, Mikos AG. Dual delivery of an angiogenic and an osteogenic growth factor for bone regeneration in a critical size defect model. Bone. 2008; 43:931–40. [PubMed: 18675385]

[177]. Watling CP, Lago N, Benmerah S, FitzGerald JJ, Tarte E, McMahon S, et al. Novel use of X-ray micro computed tomography to image rat sciatic nerve and integration into scaffold. J Neurosci Methods. 2010; 188:39–44. [PubMed: 20138083]

[178]. Faraj KA, Cuijpers V, Wismans RG, Walboomers F, Jansen JA, van Kuppevelt T, et al. Micro-computed tomographical imaging of soft biological materials using contrast techniques. Tissue Eng Part C Methods. 2009; 15:493–9. [PubMed: 19485760]

[179]. Ji C, Khademhosseini A, Dehghani F. Enhancing cell penetration and proliferation in chitosan hydrogels for tissue engineering applications. Biomaterials. 2011; 32:9719–29. [PubMed: 21925727]

[180]. Belicchi M, Cancedda R, Cedola A, Fiori F, Gavina M, Giuliani A, et al. Some applications of nanotechnologies in stem cells research. Mater Sci Eng B. 2009; 165:139–47.

[181]. Dorsey SM, Lin-Gibson S, Simon CG Jr. X-ray microcomputed tomography for the measurement of cell adhesion and proliferation in polymer scaffolds. Biomaterials. 2009; 30:2967–74. [PubMed: 19286251]

[182]. Zehbe R, Goebbels J, Ibold Y, Gross U, Schubert H. Three-dimensional visualization of in vitro cultivated chondrocytes inside porous gelatine scaffolds: a tomographic approach. Acta Biomater. 2010; 6:2097–107. [PubMed: 19931653]

[183]. Soltysiak P, Saxena AK. Micro-computed tomography for implantation site imaging during in situ oesophagus tissue engineering in a live small animal model. J Tissue Eng Regen Med. 2009; 3:573–6. [PubMed: 19685442]

[184]. Palmer AW, Guldberg RE, Levenston ME. Analysis of cartilage matrix fixed charge density and three-dimensional morphology via contrast-enhanced microcomputed tomography. Proc Natl Acad Sci U S A. 2006; 103:19255–60. [PubMed: 17158799]

[185]. Lewis RA. Medical phase contrast X-ray imaging: current status and future prospects. Phys Med Biol. 2004; 49:3573–83. [PubMed: 15446788]

[186]. Zhang L, Luo S. Micro soft tissues visualization based on X-ray phase-contrast imaging. Open Med Inform J. 2011; 5:19–25. [PubMed: 21892370]

[187]. Baruchel J, Lodini A, Romanzetti S, Rustichelli F, Scrivani A. Phase-contrast imaging of thin biomaterials. Biomaterials. 2001; 22:1515–20. [PubMed: 11374450]

[188]. Rustichelli F, Romanzetti S, Dubini B, Girardin E, Raven C, Snigirev A, et al. Phase-contrast microtomography of thin biomaterials. J Mater Sci Mater Med. 2004; 15:1053–7. [PubMed: 15448414]

[189]. Yadav PS, Kashyap Y, Sarkar PS, Sinha A, Godwal BK. Study of phase contrast imaging for carbon fiber, polystyrene and lung tissue using monochromatic and polychromatic X-ray sources. Nucl Instrum Methods Phys Res A. 2006; 564:496–505.

[190]. Appel AA, Larson JC, Somo S, Zhong Z, Spicer PP, Kasper FK, et al. Imaging of poly(alpha-hydroxy-ester) scaffolds with X-ray phase-contrast micro-computed tomography. Tissue Eng Part C Methods. 2012; 18:859–65. [PubMed: 22607529]

[191]. Zhu N, Chapman D, Cooper D, Schreyer DJ, Chen X. X-ray diffraction enhanced imaging as a novel method to visualize low-density scaffolds in soft tissue engineering. Tissue Eng Part C Methods. 2011; 17:1071–80. [PubMed: 21870940]

[192]. Thurner P, Muller B, Beckmann F, Weitkamp T, Rau C, Muller R, et al. Tomography studies of human foreskin fibroblasts on polymer yarns. Nucl Instrum Methods Phys Res B. 2003; 200:397–405.

[193]. Thurner P, Muller R, Raeber G, Sennhauser U, Hubbell JA. 3D morphology of cell cultures: a quantitative approach using micrometer synchrotron light tomography. Microsc Res Tech. 2005; 66:289–98. [PubMed: 16003782]

[194]. Albertini G, Giuliani A, Komlev V, Moroncini F, Pugnaloni A, Pennesi G, et al. Organization of extracellular matrix fibers within polyglycolic acid-polylactic acid scaffolds analyzed using X-ray synchrotron-radiation phase-contrast micro computed tomography. Tissue Eng Part C Methods. 2009; 15:403–11. [PubMed: 19326965]

[195]. Guan Y. Characterization of alginate scaffolds using X-ray imaging techniques. University of Saskatchewan. 2010

[196]. Zehbe R, Haibel A, Riesemeier H, Gross U, Kirkpatrick CJ, Schubert H, et al. Going beyond histology. synchrotron micro-computed tomography as a methodology for biological tissue characterization: from tissue morphology to individual cells. J R Soc Interface. 2010; 7:49–59. [PubMed: 19324670]

[197]. Zehbe R, Riesemeier H, Kirkpatrick CJ, Brochhausen C. Imaging of articular cartilage – data matching using X-ray tomography, SEM, FIB slicing and conventional histology. Micron. 2012; 43:1060–7. [PubMed: 22633854]

[198]. Langer M, Liu Y, Tortelli F, Cloetens P, Cancedda R, Peyrin F. Regularized phase tomography enables study of mineralized and unmineralized tissue in porous bone scaffold. J Microsc. 2010; 238:230–9. [PubMed: 20579261]

[199]. Guagliardi A, Giannini C, Cedola A, Mastrogiacomo M, Ladisa M, Cancedda R. Toward the X-ray microdiffraction imaging of bone and tissue-engineered bone. Tissue Eng Part B Rev. 2009; 15:423–42. [PubMed: 19537948]

[200]. Komlev VS, Mastrogiacomo M, Pereira RC, Peyrin F, Rustichelli F, Cancedda R. Biodegradation of porous calcium phosphate scaffolds in an ectopic bone formation model

studied by X-ray computed microtomograph. Eur Cell Mater. 2010; 19:136–46. [PubMed: 20349404]

[201]. Mastrogiacomo M, Papadimitropoulos A, Cedola A, Peyrin F, Giannoni P, Pearce SG, et al. Engineering of bone using bone marrow stromal cells and a silicon-stabilized tricalcium phosphate bioceramic: evidence for a coupling between bone formation and scaffold resorption. Biomaterials. 2007; 28:1376–84. [PubMed: 17134749]

[202]. Yeom J, Chang S, Park JK, Je JH, Yang DJ, Choi SK, et al. Synchrotron X-ray bio-imaging of bone regeneration by artificial bone substitute of MGSB and hyaluronate hydrogels. Tissue Eng Part C Methods. 2010; 16:1059–68. [PubMed: 20073984]

[203]. Wagner A, Sachse A, Keller M, Aurich M, Wetzel WD, Hortschansky P, et al. Qualitative evaluation of titanium implant integration into bone by diffraction enhanced imaging. Phys Med Biol. 2006; 51:1313–24. [PubMed: 16481696]

[204]. Cooper DML, Bewer B, Wiebe S, Wysokinski TW, Chapman D. Diffraction enhanced X-ray imaging of the distal radius: a novel approach for visualization of trabecular bone architecture. Can Assoc Radiol J. 2010; 62:251–5. [PubMed: 20591611]

[205]. Menk R, Rigon L, Arfelli F. Diffraction-enhanced X-ray medical imaging at the ELETTRA synchrotron light source. Nucl Instrum Methods Phys Res A. 2005; 548:213–20.

[206]. Sun W, Li Z-R, Yang Y-R, Shi Z-C, Wang B, Liu B, et al. Experimental study on phase-contrast imaging with synchrotron hard X-ray for repairing osteonecrosis of the femoral head. Orthopedics. 2011; 34:e530–4. [PubMed: 21902152]

[207]. Muehleman C, Fogarty D, Reinhart B, Tzvetkov T, Li J, Nesch I. In-laboratory diffraction-enhanced X-ray imaging for articular cartilage. Clin Anat. 2010; 23:530–8. [PubMed: 20544949]

[208]. Hu JZ, Wu TD, Zeng L, Liu HQ, He Y, Du GH, et al. Visualization of microvasculature by X-ray in-line phase contrast imaging in rat spinal cord. Phys Med Biol. 2012; 57:N55–63. [PubMed: 22354079]

[209]. Takeda T. Vessel imaging by interferometric phase-contrast X-ray technique. Circulation. 2002; 105:1708–12. [PubMed: 11940551]

[210]. Komlev VS, Mastrogiacomo M, Peyrin F, Cancedda R, Rustichelli F. X-ray synchrotron radiation pseudo-holotomography as a new imaging technique to investigate angio- and microvasculogenesis with no usage of contrast agents. Tissue Eng Part C Methods. 2009; 15:425–30. [PubMed: 19231984]

[211]. Brey EM, Appel A, Chiu YC, Zhong Z, Cheng MH, Engel H, et al. X-ray imaging of poly(ethylene glycol) hydrogels without contrast agents. Tissue Eng Part C Methods. 2010; 16:1597–600. [PubMed: 20662738]

[212]. Nesch I, Fogarty DP, Tzvetkov T, Reinhart B, Walus AC, Khelashvili G, et al. The design and application of an in-laboratory diffraction-enhanced X-ray imaging instrument. Rev Sci Instrum. 2009; 80:093702. [PubMed: 19791939]

[213]. Tapfer A, Bech M, Velroyen A, Meiser J, Mohr J, Walter M, et al. Experimental results from a preclinical X-ray phase-contrast CT scanner. Proc Natl Acad Sci. 2012; 109:15691–6. [PubMed: 23019354]

[214]. Hendee WR, Cleary K, Ehman RL, Fullerton GD, Grundfest WS, Haller J, et al. Bioengineering and imaging research opportunities workshop V: a summary on imaging and characterizing structure and function in native and engineered tissues. Cytometry A. 2008; 73:779–84. [PubMed: 18677767]

[215]. Chouinard JA, Rousseau JA, Beaudoin JF, Vermette P, Lecomte R. Positron emission tomographydetection ofhuman endothelial cell and fibroblast monolayers: effect of pretreatment and cell density on 18FDG uptake. Vasc Cell. 2012; 4:5. [PubMed: 22433292]

[216]. Nieuwoudt M, Wiggett S, Malfeld S, van der Merwe SW. Imaging glucose metabolism in perfluorocarbon-perfused hepatocyte bioreactors using positron emission tomography. J Artif Organs. 2009; 12:247. [PubMed: 20035398]

[217]. Kofidis T, Lenz A, Boublik J, Akhyari P, Wachsmann B, Mueller-Stahl K, et al. Pulsatile perfusion and cardiomyocyte viability in a solid three-dimensional matrix. Biomaterials. 2003; 24:5009–14. [PubMed: 14559014]

[218]. Mertsching H, Walles T, Hofmann M, Schanz J, Knapp WH. Engineering of a vascularized scaffold for artificial tissue and organ generation. Biomaterials. 2005; 26:6610–7. [PubMed: 15979139]

[219]. Walles T, Giere B, Hofmann M, Schanz J, Hofmann F, Mertsching H, et al. Experimental generation of a tissue-engineered functional and vascularized trachea. J Thorac Cardiovasc Surg. 2004; 128:900–6. [PubMed: 15573075]

[220]. Srinivas M, Aarntzen EH, Bulte JW, Oyen WJ, Heerschap A, de Vries IJ, et al. Imaging of cellular therapies. Adv Drug Deliv Rev. 2010; 62:1080–93. [PubMed: 20800081]

[221]. Kempen DH, Yaszemski MJ, Heijink A, Hefferan TE, Creemers LB, Britson J, et al. Non-invasive monitoring of BMP-2 retention and bone formation in composites for bone tissue engineering using SPECT/CT and scintillation probes. J Control Release. 2009; 134:169–76. [PubMed: 19105972]

[222]. Zhou J, Lin H, Fang T, Li X, Dai W, Uemura T, et al. The repair of large segmental bone defects in the rabbit with vascularized tissue engineered bone. Biomaterials. 2010; 31:1171–9. [PubMed: 19880177]

[223]. Bai F, Wang Z, Lu J, Liu J, Chen G, Lv R, et al. The correlation between the internal structure and vascularization of controllable porous bioceramic materials in vivo: a quantitative study. Tissue Eng Part A. 2010; 16:3791–803. [PubMed: 20673021]

[224]. Bai F, Zhang J, Wang Z, Lu J, Chang J, Liu J, et al. The effect of pore size on tissue ingrowth and neovascularization in porous bioceramics of controlled architecture in vivo. Biomed Mater. 2011; 6:1–10.

[225]. Terrovitis J, Lautamaki R, Bonios M, Fox J, Engles JM, Yu J, et al. Noninvasive quantification and optimization of acute cell retention by in vivo positron emission tomography after intramyocardial cardiac-derived stem cell delivery. J Am Coll Cardiol. 2009; 54:1619–26. [PubMed: 19833262]

[226]. Tran N, Maskali F, Franken P, Nloga J, Lahoutte T, Maureira P, et al. In vivo location of intramyocardial implanted 111in-oxine labeled mesenchymal stem cells: assessment with dual energy pinhole 99mTc-SestaMIBI SPECT in a rat model of myocardial infarction. J Heart Lung Transplant. 2005; 24:S136–7.

[227]. Lin C-Y, Lin K-J, Li K-C, Sung L-Y, Hsueh S, Lu C-H, et al. Immune responses during healing of massive segmental femoral bone defects mediated by hybrid baculovirus-engineered ASCS. Biomaterials. 2012; 33:7422–34. [PubMed: 22796166]

[228]. Ritman EL. Micro-computed tomography-current status and developments. Annu Rev Biomed Eng. 2004; 6:185–208. [PubMed: 15255767]

[229]. Cronin M, Akin AR, Collins SA, Meganck J, Kim JB, Baban CK, et al. High resolution in vivo bioluminescent imaging for the study of bacterial tumour targeting. PloS ONE. 2012; 7:e30940. [PubMed: 22295120]

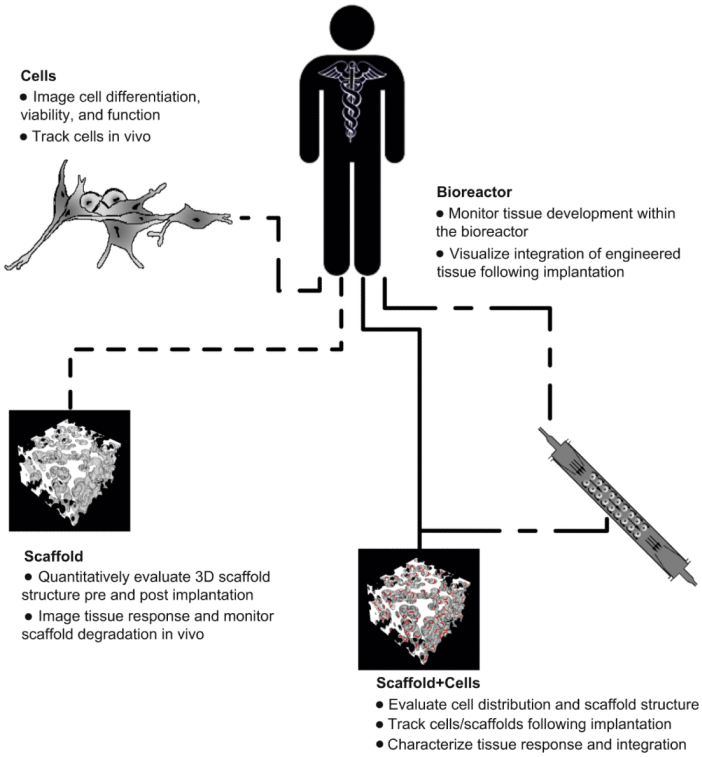

Fig. 1.
Schematic of TERM strategies along with identified imaging needs associated with each.

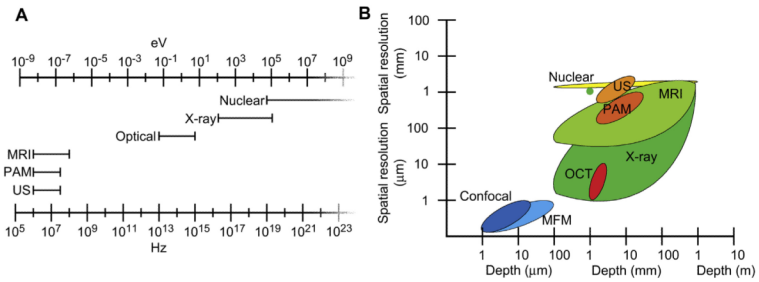

Fig. 2.

(A) Range of energies/frequencies on the electromagnetic spectrum used by 3D imaging modalities. (B) Approximate ranges of spatial resolution and imaging depth achievable by imaging modalities. US = ultrasound, PAM = photoacoustic microscopy, MRI = magnetic resonance imaging, MFM = multiphoton fluorescence microscopy, OCT = optical coherence tomography.

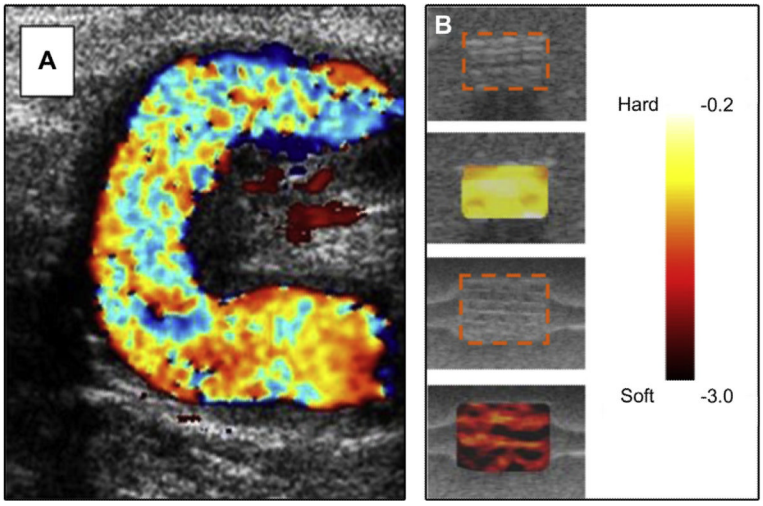

Fig. 3.

Examples of ultrasound images produced for TERM applications. (A) Color image of flow in a tissue engineered vascular graft. Figure reproduced with permission, from Tillman et al. [6]. (B) Strain maps overlaid on a B-scan before (top two) and after (bottom two) degradation showing changes in mechanical properties *in vitro*. Figure reproduced with permission, from Kim et al. [21].

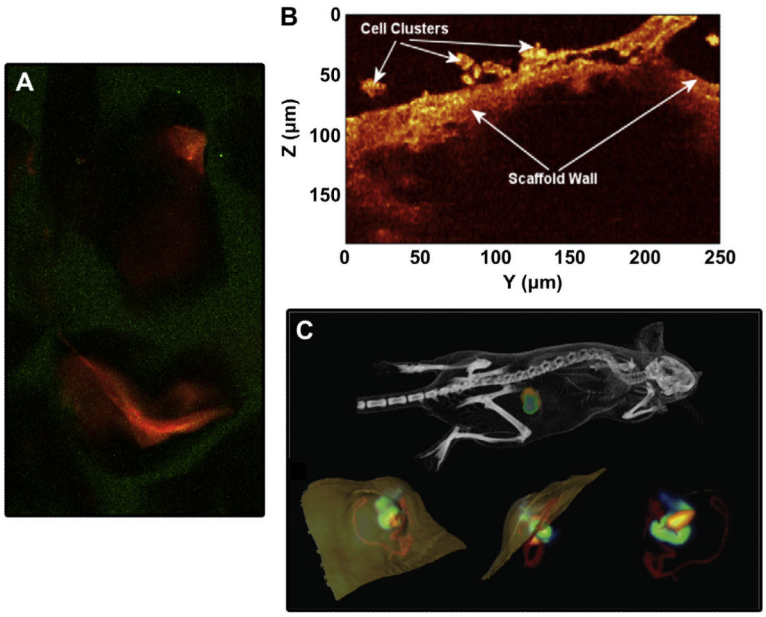

Fig. 4.

Images of biomaterials, cells, and tissue structure generated using optical imaging techniques. (A) Fluorescent image of porous synthetic hydrogel that exhibits auto-fluorescence (green) loaded with fluorescently tagged fibrin (red). (B) OCT images of a biomaterial scaffolds seeded with MG63 bone cells. Figure reproduced with permission from IOP publishing from Yang et al. http://dx.doi.org/10.1088/0031-9155/51/7/001 [46]. (C) Combined luminescence and μCT demonstrating co-localization of bacteria (orange) and a subcutaneous tumor (green) within the animal. Lower images show a magnification the tumor from mouse: showing regions of tumor (FLuc green/blue), vasculature (contrast agent – red) and bacterial (orange/yellow) signals. Figure reproduced with permission, from Cronin et al. [229]. (For interpretation of the references to colour in this figure legend, the reader is referred to the web version of this article.)

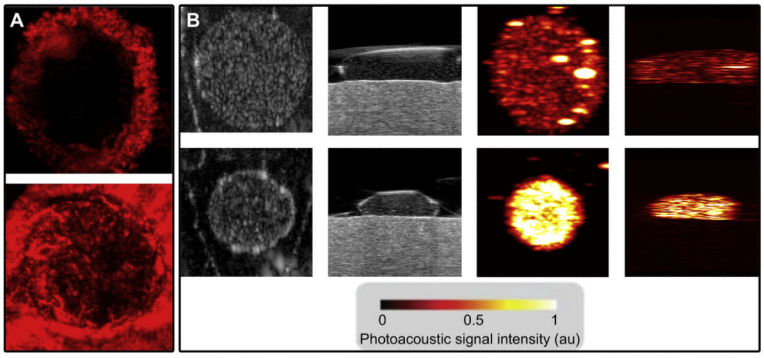

Fig. 5.

Examples of photoacoustic and PAM/US images from TERM applications. (A) PAM images revealing neovasculature in a porous scaffold at 1 (top) and 6 (bottom) weeks post-implantation. Images produced using the same methods described in Cai et al. [82]. (B) Dual ultrasound (left) and photoacoustic (right) imaging of adipose-derived stem cells in a fibrin gel at days 1 (top) and 16 (bottom). Images produced using the same methods described in Chung et al. [86].

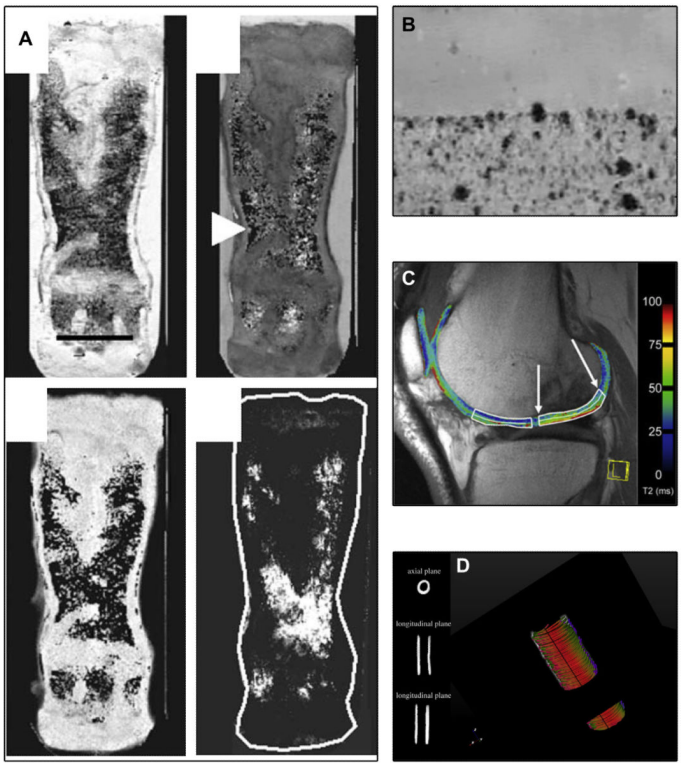

Fig. 6.

Examples of MRI images from TERM applications. (A) Four different MRI contrast mechanism images of a 38-week phalange model. Figure reproduced with permission, from Potter et al. [94]. (B) *In vitro* MR imaging of collagen hydrogels loaded with mesenchymal stem cells. Differences in signal are observed between scaffolds with labeled cells (bottom) versus unlabeled cells (top). Figure reproduced with permission, from Heymer et al. [109]. (C) Depiction of cartilage in a patient 6 months after chondrocyte transplantation. Arrows mark the area of cartilage repair. Figure reproduced with permission, from Welsch et al. [120]. (D) Fiber trajectories obtained by DTI representing collagen fibers in an artery: red (*x*-direction), green (*y*-direction) and blue (*z*-direction). Figure reproduced with permission, from Ghazanfari et al. [133]. (For interpretation of the references to colour in this figure legend, the reader is referred to the web version of this article.)

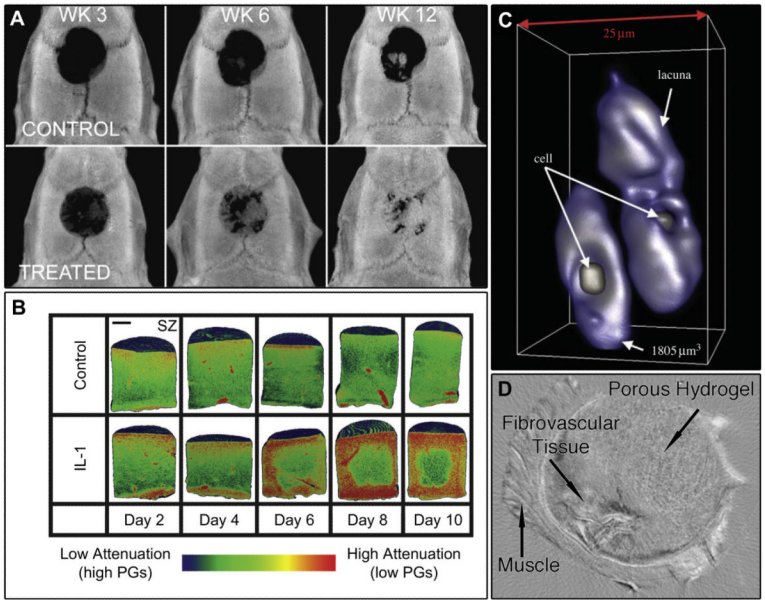

Fig. 7.

Example of X-ray images from TERM applications. (A) µCT images showing bone regeneration in cranial defects in response to growth factor treatment over time. Figure reproduced with permission from IOP publishing from Umoh et al. http://dx.doi.org/10.1088/0031-9155/54/7/020 [169]. (B) EPIC-µCT in an *in vitro* cartilage degradation model. Representative 3D EPIC-µCT images of control and IL-1-stimulated explants demonstrating progressive increases in attenuation in treated samples. Figure reproduced with permission, from Palmer et al. [184]. (C) Cell structures imaged in the soft tissue region of articular cartilage. Figure reproduced with permission, from Zehbe et al. [196]. (D) X-ray PC CT of explanted hydrogels implanted adjacent to skeletal muscle. The fibrovascular tissue, muscle and hydrogel can be identified.

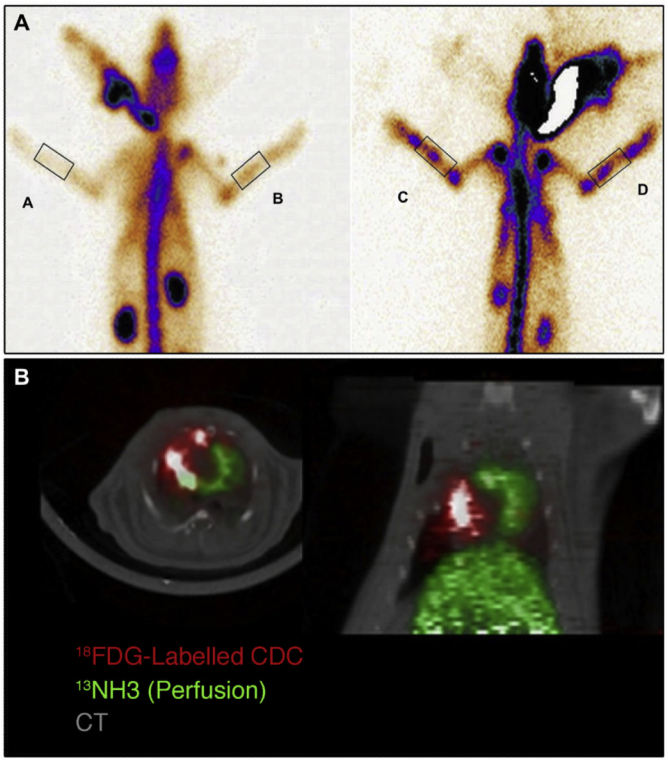

Fig. 8.

Examples of nuclear imaging in TERM applications: (A) SPECT 12 weeks postoperative showing activity in scaffolds seeded with cells (C and D) versus defects with no cells (A and B). Figure reproduced with permission, from Zhou et al. [222]. (B) Transverse and coronal fusion of computed tomography (CT) and micro-positron computed tomography (PET) images showing the distribution of ^{18}FDG labeled cells injected in the myocardium. Figure reproduced with permission, from Terrovitis et al. [225].